Physical controls of near-surface soil moisture across varying spatial scales in an agricultural landscape during SMEX02

Champa Joshi[1] and Binayak P. Mohanty[1]

Received 28 January 2010; revised 3 September 2010; accepted 28 September 2010; published 2 December 2010.

[1] Understanding of near-surface soil moisture variability at different spatial scales and associated dominant physical controls is limited. In the past, soil moisture dynamics studies have been conducted extensively at different spatial scales using both in situ and remote sensing (RS) data in the subhumid Southern Great Plains region, which has mostly pasture and range land cover with rolling topography. Compared to the past efforts, we investigated the space-time characterization of near-surface soil moisture and associated physical controls at multiple scales (field, watershed, and region) in a humid hydroclimatic region with different topography and agricultural land cover. Soil moisture data from two different measurement support scales (theta probe based (point scale) and airborne RS derived; footprint scale, 800 m × 800 m), obtained during the Soil Moisture Experiment 2002 (SMEX02) in Iowa were used. Geostatistical analysis showed the spatial soil moisture correlation lengths varied between 78 m and 307 m (at the field scale), 2044 m and 11,882 m (at the watershed scale), and 19,500 m and 118,500 m (at the regional scale). The correlation length values were usually smaller on wet days than the relatively dry days at the field and watershed scales. The trend was opposite at the regional scale with correlation lengths being larger on wet days. Furthermore, the soil moisture data sets were decomposed into spatial Empirical Orthogonal Function (EOF) patterns, and their relationship with various geophysical parameters (rainfall, topography, soil texture, and vegetation) was examined to determine the dominant control on the near-surface soil moisture variability. At the field scale, the first *four* EOFs together explained about 81% of the total variability. At the watershed scale, the first *two* EOFs were dominant explaining about 93% of the total variance, whereas at the regional scale, the primary EOF itself explained more than 70% of the variance. In other words, the complicated dynamics of near-surface soil moisture fields can be described by a few underlying orthogonal spatial structures related to the geophysical attributes of the region. Correlation analysis of the RS soil moisture data showed that rainfall, topography, and soil texture have mixed effects on the variability explained by the dominant EOFs, at both watershed and regional scales, with limited influence of vegetation parameters. The effect of rainfall on the soil moisture variability is higher at the watershed scale compared to the regional scale in Iowa.

Citation: Joshi, C., and B. P. Mohanty (2010), Physical controls of near-surface soil moisture across varying spatial scales in an agricultural landscape during SMEX02, *Water Resour. Res.*, *46*, W12503, doi:10.1029/2010WR009152.

1. Introduction

[2] Near-surface soil moisture is a key state variable of the water cycle as it plays a significant role in the global water and energy balance by affecting several hydrological, ecological, meteorological, geomorphologic, and other natural processes. Soil moisture varies greatly across space and time based on different soil properties, topographic features, vegetation characteristics, and atmospheric dynamics [*Famiglietti et al.*, 1999; *Entin et al.*, 2000; *Mohanty and Skaggs*, 2001]. Soil moisture is either measured directly using in situ methods, e.g., gravimetric sampling, time domain reflectrometry (TDR) [*Grayson and Western*, 1998; *Mohanty et al.*, 1998], or estimated indirectly through *active* [*Dubois et al.*, 1995; *De Troch et al.*, 1996; *Ulaby et al.*, 1996] or *passive* [*Jackson*, 1993; *Jackson and Schmugge*, 1995; *Jackson and Le Vine*, 1996; *Schmugge*, 1998; *Njoku et al.*, 2003] remote sensing (RS) techniques. As in situ measurements have small support, therefore, for estimation of soil moisture fields at larger spatial scales, we rely greatly on the RS methods. However, the passive microwave RS sensors have limited penetration depths, ranging from ~5 cm for the low-frequency L band, to a few mm for the high-frequency X band radiometry [*Kerr*, 2007]. Nevertheless,

[1]Department of Biological and Agricultural Engineering, Texas A&M University, College Station, Texas, USA.

Copyright 2010 by the American Geophysical Union.
0043-1397/10/2010WR009152

the spatial resolution of remotely sensed soil moisture footprints very often conflicts with the needs of the scientific or research community, necessitating the use of down-/up-scaling algorithms to render the data suitable for various applications (e.g., large-scale general circulation models (GCMs), weather forecast models, hydrologic models, or precision agriculture) [*Dubayah et al.*, 1997; *Drusch and Wood*, 1999; *Crow and Wood*, 2002; *Kim and Barros*, 2002a; *Merlin et al.*, 2006, 2008]. Therefore, knowledge of spatiotemporal variability of soil moisture patterns and their evolution across widely ranging scales of both space and time, along with the geophysical parameters (e.g., topography, rainfall, soil texture, and vegetation) controlling the variability, is crucial for numerous hydrological research and applications, such as flood/drought prediction, climate forecast modeling, and agricultural management practices [*Gordon and Hunt*, 1987; *Crow and Wood*, 2002; *Delin and Berglund*, 2005; *Starr*, 2005]. In particular, a better understanding of the variability of RS soil moisture, will help evaluate the passive microwave sensor performance, thereby, increasing the quality and credibility of the RS data. It will also help to quantify the variability underlying large-scale RS averaged soil moisture data that the sensor fails to capture explicitly which in turn will increase the usage of the data in scientific/research community [*Famiglietti et al.*, 1999]. Knowledge of the various geophysical controls affecting the RS soil moisture variability at varying spatial scales (e.g., watershed and regional scales) can also help to improve the performance of soil moisture retrieval algorithm by decreasing the uncertainty in assigning proper weights to the various geophysical parameters involved in the derivation of the moisture estimates.

[3] In the past, soil moisture characterization studies using ground-based soil moisture measurements have focused mostly on small scales [e.g., *Hills and Reynolds*, 1969; *Charpentier and Groffman*, 1992; *Famiglietti et al.*, 1999; *Mohanty et al.*, 2000], while those using RS soil moisture data encompassed larger spatial scales [e.g., *Hu et al.*, 1997; *Kim and Barros*, 2002b; *Ryu and Famiglietti*, 2006; *Jawson and Niemann*, 2007]. Though it is easy to calibrate the ground-based measurements, but they cover small areas, thereby, limiting the spatial correlation analysis of soil moisture due to the small number of measurements [*Western et al.*, 1998]. On the other hand, RS soil moisture measurements provide data over larger spatial extents, but the interpretation poses a challenge, especially for surfaces having vegetative cover. The footprint often results in significant smoothing of the small-scale variability present in near-surface soil moisture [*Western et al.*, 2004].

[4] To study the space-time characterization of soil moisture patterns, two different techniques widely used by hydrologists are the *geostatistical* method [*Journel and Huijbregts*, 1978], and the *Empirical Orthogonal Function* (*EOF*) analysis [*Preisendorfer*, 1988]. Standard geostatistical techniques involve the estimation of isotropic/directional semivariograms to understand the spatial structure of soil moisture and determining the correlation lengths at different sampling scales. The correlation length is a measure of the spatial continuity of the soil moisture. The sample variogram calculated from the soil moisture data gives information about the sample properties only. The properties of the true population (or the underlying soil moisture distribution) are then statistically determined by fitting a theoretical variogram model to the sample variogram. Whether the variogram parameters (i.e., the sill, nugget, and range/correlation length) determined from the sample truly represent the population depends on the nature of the soil moisture variability and the sampling regime [*Western et al.*, 1998].

[5] Literature contains a wealth of information where geostatistical method was used to study the spatial structure and correlation lengths of soil moisture, both at small and large spatial scales. Results obtained from various studies are of conflicting nature. Some authors [*Schmugge and Jackson*, 1996; *Charpentier and Groffman*, 1992; *Hills and Reynolds*, 1969] found little evidence, while several others [*Warrick et al.*, 1990; *Nyberg*, 1996; *Western et al.*, 1998] observed the presence of spatial correlations in soil moisture. However, their studies differ from each other depending on the methods employed for data collection, the support scale, and the depth to which the soil moisture measurements were recorded. While *Schmugge and Jackson* [1996] used RS soil moisture estimates with a larger support scale in their study, other authors used in situ measured point-scale data. Furthermore, works of *Schmugge and Jackson* [1996], *Charpentier and Groffman* [1992], and *Hills and Reynolds* [1969] focus on the near-surface soil moisture, whereas *Warrick et al.* [1990], *Nyberg* [1996], and *Western et al.* [1998] used profile soil moisture up to a depth of about 15–30 cm from soil surface. From soil moisture data (~0–8 cm) collected over a range of scales in Chew Stoke catchment (UK), *Hills and Reynolds* [1969] inferred that the soil moisture variability increased significantly with scale, suggesting the presence of spatial correlation. *Western et al.* [1998] conducted the geostatistical characterization of soil moisture patterns (top 30 cm) in the 10.5 ha Tarrawarra catchment in Australia on 13 occasions. Using TDR, they measured soil moisture between 500 and 2000 points for each occasion and analyzed the spatial correlation structure. They found the sample variograms with a clear sill and nugget and observed that the geostatistical structure of soil moisture evolved seasonally. During the wet winter period, high sills (15–25 $(\%v/v)^2$) and low correlation lengths (35–50 m) were observed, whereas in the dry summer period sills were smaller (5–15 $(\%v/v)^2$) and correlation lengths longer (50–60 m). They concluded that this seasonal evolution is based on the lateral redistribution of soil moisture during different seasons. *Mohanty et al.* [2000] analyzed the spatial structure of near-surface soil moisture (0–6 cm) in a mixed vegetation pixel during the Southern Great Plains 1997 (SGP97) hydrology experiment. They explored the within-season spatiotemporal variability of surface soil moisture in a 800 m × 800 m field (LW21) having a relatively uniform topography and soil texture, but variable land cover. Their analyses showed the effects of daily precipitation, variable land cover, land management, vegetation growth, and microheterogeneity on soil moisture distribution. Isotropic correlation length for soil moisture varied between <100 m (for nugget and subgrid-scale variability) and >428 m (for spherical and Gaussian models reflecting contribution from coexisting geophysical processes). Analysis of spatial structure at other scales up to 10 km using the RS soil moisture (Electronically Scanned Thinned Array Radiometer, ESTAR-derived) fields (soil depth ~top 5 cm; resolution ~200 m × 200 m) from the Washita '92 campaign [*Jackson et al.*, 1995] exhibited fractal behavior [*Hu et al.*, 1997]. Using the same data set, *Cosh and Brutsaert* [1999]

subdivided an 18 km × 25 km study region in to 32 block grids consisting of 200 m × 200 m pixels; and concluded that for distances <5 km, the surface soil moisture exhibited spatial correlation with correlation length of approximately 1 km. Based on their analysis for each of the individual soil types over the entire Washita '92 region, they observed similar correlation length with the soil moisture variability being strongly affected by the soil type. *Ryu and Famiglietti* [2006] investigated the scaling behavior of near-surface soil moisture spatial variance with increasing support scale (1×1 km^2 to 140×140 km^2) using SGP97 ESTAR data in a 50 km × 250 km region of central Oklahoma. They observed a nested correlation structure within regional-scale fields, with the smaller-scale correlation (10 ~ 30 km) governed by land surface features (soil texture and vegetation), and larger-scale correlation (60 ~ ≥100 km) by precipitation. They further concluded that at the larger scales (considered in their study), the type of correlation function and correlation length are significant in determining the relationship between soil moisture variance and support area, and the variance no longer follows a power law decay rule with increasing support area as it does at smaller scales (<1 km^2). The differences in correlation length between small-scale and large-scale studies may be due to the effects of sampling design [*Western and Blöschl*, 1999] and the uncertainty associated with sampling [*Western et al.*, 1998]. Geophysical process controls also change with changes in spatial scale leading to differences in correlation lengths [*Western et al.*, 2004].

[6] The EOF analysis [*Preisendorfer*, 1988] has also been extensively used to study spatial patterns and the ensuing dynamics of soil moisture. The method essentially generates orthogonal spatial patterns called 'EOFs' (invariant in time), and a set of time series referred to as 'Principal Components' or 'PCs' (invariant in space), of the soil moisture anomalies. The method computes the amount of variance explained by different modes of variability (i.e., each EOF/PC pair). The primary EOF/PC pair explains the maximum amount of variance. The EOF method is also used to investigate which regional geophysical characteristics (e.g., topography, soil texture, vegetation) control the EOF patterns.

[7] *Kim and Barros* [2002b] explored the statistical structure of large-scale (40 km × 250 km) soil moisture fields obtained during the SGP97 hydrology experiment. The EOF analysis was used to determine the relationship between the spatial structure of soil moisture and the available ancillary data (topography, soil texture, and vegetation cover). They observed that topography dominated the spatial structure of soil moisture only during and immediately after a rainfall event. In interstorm periods, the spatial evolution of soil moisture was associated mainly with the soil hydraulic properties when the soil was above field capacity, while vegetation dominated soil moisture evolution during the dry down period. *Yoo and Kim* [2004] investigated the spatio-temporal variability of field-scale soil moisture using gravimetric soil moisture data from two Little Washita fields (LW10 and LW13) during SGP97. They evaluated the relative roles of various factors (topography, soil properties, and vegetation) and concluded that there is no simple and unique mechanism that can be applied to explain the evolution of soil moisture field. Even though topography was found to be dominant, other factors such as soil and land use were also significant in controlling the spatial organization of soil moisture content. *Jawson and Niemann* [2007] used EOF approach to show that the spatial and temporal variation of large-scale soil moisture patterns can be described by a small number of spatial structures related to soil texture, topography, and land use. They analyzed the spatial and temporal anomalies computed from the ESTAR based soil moisture data set from SGP97, and found that one spatial EOF pattern explained most of the variance in both the spatial and temporal cases. They further concluded that the spatial structures (EOFs) of both the spatial and temporal anomalies were mostly correlated with the soil texture, whereas the effects of topography were relatively insignificant for the range of spatial scales considered in their study. *Perry and Niemann* [2007] examined the soil moisture data set obtained from the Tarrawara catchment in Australia. They concluded that the spatial patterns are controlled by local soil properties in wet and dry conditions and by topography during the intermediate period.

[8] The primary objective of this study is to investigate the space-time variability and the associated dominant physical control(s) of near-surface soil moisture at varying spatial scales in an agricultural landscape in Iowa. Compared to the works by *Yoo and Kim* [2004] and *Jawson and Niemann* [2007] in the SGP region, Oklahoma, this study is focused on the soil moisture patterns at multiple spatial scales (field, watershed, and region) in a different hydroclimatic (humid climate, gentle terrain, agricultural landscape, and glacial till soil) region.

2. Study Site and Data Description

[9] Figure 1 shows the regional study area of the SMEX02 campaign in Iowa (including the insets of 100 km^2 Walnut Creek (WC) watershed and the 800 m × 800 m WC11 field) located south of Ames, Iowa. The climate of the region is mostly humid, with an average annual precipitation of 835 mm. The heaviest rainfall usually occurs in May and June and amounts to about one third of the annual total. The regional topography consists of low relief (maximum elevation ~320 m) with poor surface drainage due to the existing prairie potholes of glacial origin. Soil texture varies considerably from fine sandy loam to clay, with the majority classified as silt loam with a relatively low permeability. Corn (50%) and soybean (40%) crops dominate the land cover with row type cultivation [*Choi and Jacobs*, 2007].

[10] The SMEX02 field campaign took place in Iowa from 25 June to 12 July 2002. A detailed description of this campaign including the mission objectives, experiment plan, site description can be found at URL http://hydroloab.arsusda.gov/smex02. During SMEX02, ground-based soil moisture measurements were done for 12 days at 92 sampling points in the WC11 field. Measurements were conducted between 1100 and 1500 local time (CDST). Sampling points were located at nearly 30 m intervals along the four transects oriented east–west (EWN and EWS) and north–south (NSE and NSW) within the field (Figure 1). The volumetric soil moisture contents were measured using 6 cm long theta probes and data loggers (ML-2 probes and HH2 data loggers of Delta-T Inc.; http://www.delta-t.co.uk). During SMEX02, the WC11 field had a corn crop cover with a small patch of soybean planted near the western edge of the field. The soil texture of the field consists of 24.5%

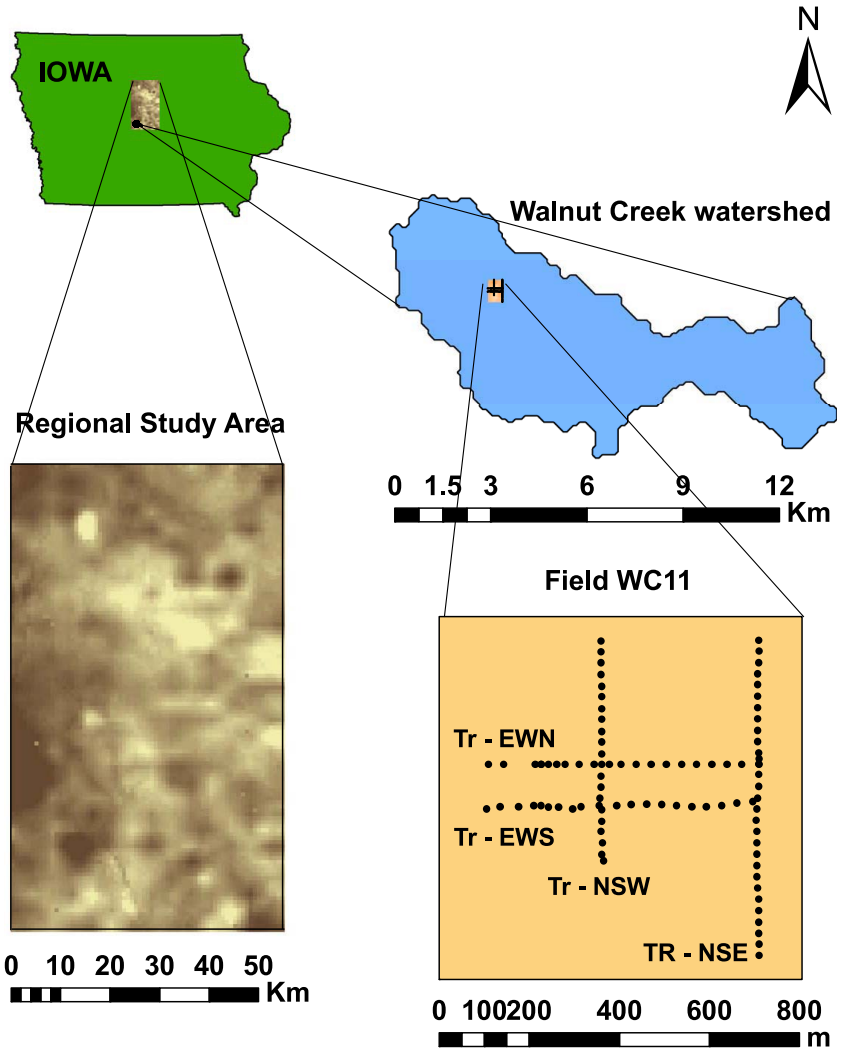

Figure 1. The SMEX02 regional study area including the WC watershed and the WC11 field in Iowa. Transects (EWN, EWS, NSE, and NSW) within the WC11 field indicate soil moisture sampling locations.

sand and 28.6% clay. The dimension of the WC11 field (800 m × 800 m) is similar to the resolution of an airborne remote sensor footprint. However, for analysis purposes at the field scale, only the sampling domain (effective size ~700 m × 455 m) consisting of the four transects (see Figure 1) was considered.

[11] The airborne Polarimetric Scanning Radiometer (PSR) observations (resolution: 800 m × 800 m, regional coverage: 144 × 70 pixels) were collected for 10 days, between 25 June and 12 July, during SMEX02. The PSR is an airborne microwave imaging radiometer developed and operated by the National Oceanic and Atmospheric Administration (NOAA) Environmental Technology Laboratory [*Piepmeier and Gasiewski*, 2001]. During the campaign, PSR used various frequencies (6.0 GHz, 6.5 GHz, 6.92 GHz, 7.32 GHz, 10.64 GHz, 10.69 GHz, 10.70 GHz, 10.75 GHz and thermal) for passive microwave remote sensing [*Bindlish et al.*, 2006; *Das and Mohanty*, 2008]. *Bindlish et al.* [2006] examined the effects of Radio Frequency Interference (RFI) and suggested that the 7.32 GHz and 10.70 GHz bands were far superior to the other PSR frequencies. Therefore, the soil moisture fields of the SMEX02 region were created using these two PSR/CX band channels. During the experiment, the vegetation conditions were close to peak biomass conditions (~8 kg/m^2). *Bindlish et al.* [2006] developed a soil moisture retrieval algorithm similar to one proposed by *Jackson* [1993] to account for the nonlinear relationship between brightness temperature, soil moisture, surface roughness and vegetation water content. In addition to the sensor-measured brightness temperature, their algorithm requires several ancillary data sets for implementation, such as, surface soil texture, land cover, and Normalized Difference Vegetation Index (NDVI). The sensor measurements were validated against 42 theta probe readings from 14 different locations and 4 gravimetric soil moisture (GSM) samples (coincident with 4 theta probe locations) taken in every field across the WC watershed area. However, the penetration depth of the high-frequency PSR/CX band channels is low compared to the top 6 cm of the surface soil layers sensed by the theta probe instrument. At the field scale, the PSR soil moisture estimates have a standard error of estimate (SEE) of 5.5%. At coarser

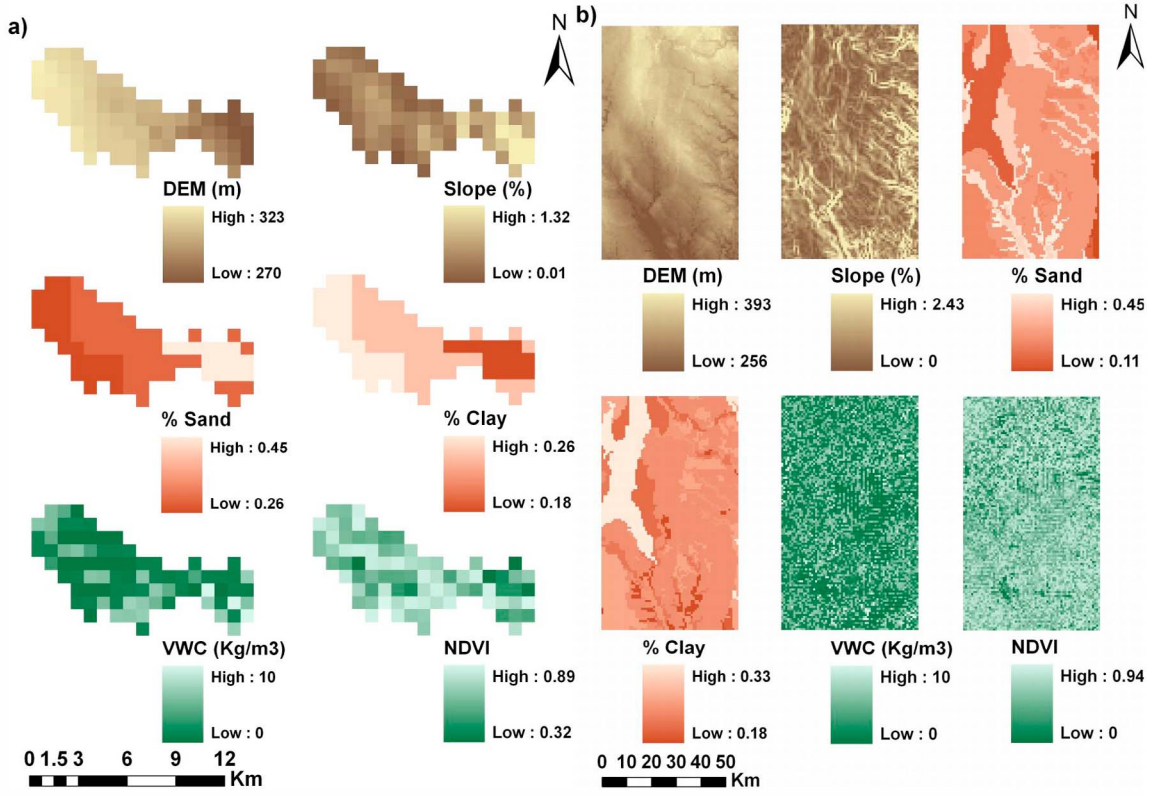

Figure 2. Topographic, soil, and vegetation attributes of (a) the WC watershed and (b) the SMEX02 regional site, during the SMEX02 campaign (resolution ~800 m × 800 m).

resolution (~25 km), the errors dropped considerably with SEE = 2.85%. For analysis purposes, the null values present near the bottom portion of the PSR-derived regional soil moisture fields were discarded by trimming the moisture fields to a net size of 118 × 69 pixels (i.e., 94,400 m × 55,200 m) of 800 m × 800 m resolution. The WC watershed consists of 84 pixels of similar resolution.

[12] To conduct the correlation analysis for exploring the relationship between the various regional characteristics and the spatial variability of soil moisture fields at the watershed and the regional scales, the digital elevation model (DEM) (USGS GTOPO30 data: resolution ~1 km × 1 km), slope (derived from DEM), vegetation water content (VWC) (Landsat Imagery; resolution ~30 m), NDVI (Landsat Imagery; resolution ~30 m), percent sand and percent clay in the soils (derived from CONUS-SOIL data set; resolution ~1 km × 1 km) were used. The DEM, slope, VWC, NDVI, percent sand and percent clay data were normalized using the corresponding mean and standard deviation for correlation analysis. Figures 2a and 2b show the topographic, soil, and vegetation attributes for the WC watershed and the SMEX02 regional site, respectively. The precipitation information comes from the Soil Climate Analysis Network (SCAN) site in Ames for the field-scale analysis, while at the watershed and the regional scales, the NEXRAD data (resolution: 4 km × 4 km) were used. Figures 3a and 3b show the precipitation evolution map of the watershed and the regional site, respectively. All the ancillary data sets (DEM, slope, VWC, NDVI, CONUS-based soil data, and NEXRAD-precipitation) were aggregated/disaggregated to a spatial resolution of 800 m × 800 m to match with the resolution of the PSR pixels. The RS soil moisture images as well as the ancillary data sets were georeferenced and projected in the WGS84 UTM Zone 15 coordinate system for analyses purpose.

3. Methods

3.1. Variogram Analysis

[13] To study the evolution of spatial structure of near-surface soil moisture with time, at varying spatial scales (i.e., field, watershed, and regional scales), we conducted a variogram analysis using standard geostatistical techniques [*Journel and Huijbregts*, 1978; *Issaks and Srivastava*, 1989; *Mohanty et al.*, 2000; *Wackernagel*, 2003]. The analysis involves calculating the experimental (or sample) semivariogram for the soil moisture fields obtained for each sampling date, and thereafter, fitting a theoretical semivariogram model to the experimental semivariogram. The traditional semivariogram estimator, $\gamma^*(h_i)$ is defined as

$$\gamma^*(h_i) = \frac{1}{2N(h_i)} \sum_{i=1}^{N(h_i)} [\theta(z) - \theta(z + h_i)]^2 \quad (1)$$

where $N(h_i)$ is the number of pairs of soil moisture measurements $[\theta(z), \theta(z + h_i)]$ separated by a lag range h_i. As semivariogram is a function of both lag distance and direction (resulting in directional/anisotropic semivariograms), we have considered only the isotropic semivariograms for the present study, ignoring the directional ones. The isotropic

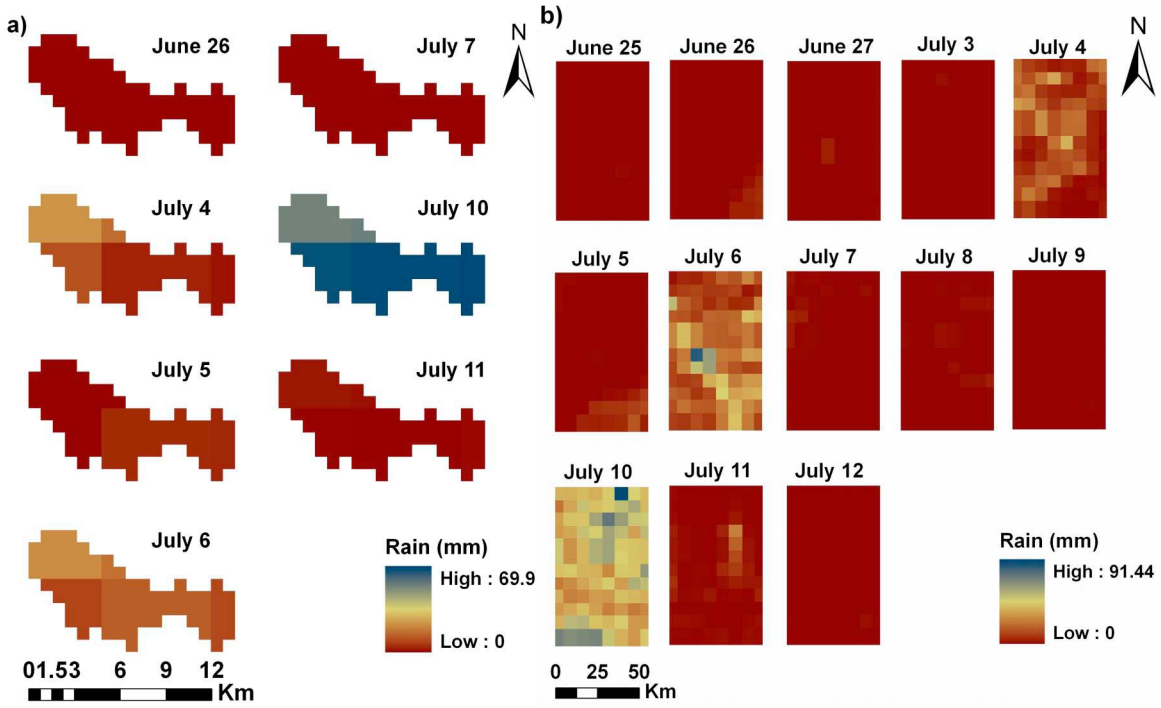

Figure 3. Precipitation evolution map of (a) the WC watershed and (b) the SMEX02 regional site, during the SMEX02 campaign (resolution ~800 m × 800 m).

semivariograms for the theta probe measurements as well as the PSR-derived remotely sensed soil moisture fields were estimated using geostatistical software, GS$^+$ (Gamma Design Software, Plainwell, Michigan). Lag distances were grouped for producing semivariogram estimations with reasonably large number of data pairs at both the watershed and regional scales. Using a nonlinear least squares technique, three different theoretical semivariogram (spherical, exponential and Gaussian) models were fitted to the isotropic experimental semivariograms, for quantifying the geostatistical structure of the theta probed measured and PSR-derived soil moisture patterns. A brief description of these theoretical models is given below.

Spherical isotropic model

$$\gamma(h) = \begin{cases} C_0 + C\left[1.5(h/A_0) - 0.5(h/A_0)^3\right] & h \le A_0 \\ C_0 + C & h > A_0 \end{cases} \quad (2)$$

Exponential isotropic model

$$\gamma(h) = C_0 + C[1 - \exp(-h/A_0)] \quad (3)$$

Gaussian isotropic model

$$\gamma(h) = C_0 + C\left[1 - \exp\left(-h^2/A_0^2\right)\right] \quad (4)$$

where $\gamma(h)$ is the semivariance for lag h, h is the lag interval, C_0 is the nugget variance, C is the structural variance, and A_0 is the correlation range parameter.

[14] For a spherical model, the effective range (or the spatial correlation length) is the same as the range parameter A_0, whereas for a Gaussian and an exponential model, the effective range is $3^{0.5}A_0$ and $3A_0$, respectively. For further details, readers may refer to the standard geostatistics texts [*Journel and Huijbregts*, 1978; *Cressie*, 1993; *Wackernagel*, 2003].

3.2. Empirical Orthogonal Function Analysis

[15] The Empirical Orthogonal Function (EOF) analysis, also referred to as the Principal Component Analysis (PCA), is a statistical tool used for analyzing the spatial or temporal variability of geophysical fields [*Preisendorfer*, 1988]. The EOF analysis aims to reduce the dimensionality of a data set consisting of a large number of correlated variables, while preserving maximum possible variability present in the data set. This is done by transforming the original data set into a new set of uncorrelated variables, ordered so that the first few of the new variables explain most of the variation existing in the original data set [*Jolliffe*, 2002].

[16] For a spatiotemporal soil moisture data set, the EOF method can be used to decompose the observed soil moisture variability into a set of orthogonal spatial patterns (called EOFs), which are invariant in time, and a set of time series (termed as Principal Components or PCs), which are invariant in space. For EOF analysis, we used the spatial anomalies of soil moisture data set obtained from the theta probe measurements and the PSR sensor during the SMEX02 campaign. Using spatial anomalies instead of the soil moisture excludes the temporal variation from consideration [*Perry and Niemann*, 2007]. The spatial anomalies are calculated by subtracting the mean soil moisture for a given sampling day from all the soil moisture observations collected on that day. Thus, the spatial anomaly $x_i(t)$ at a location i at time t can be defined as

$$x_i(t) = s_i(t) - \frac{1}{m}\sum_{j=1}^{m} s_j(t) \quad (5)$$

Table 1. Summary of Theta Probe Measured Soil Moisture Data in the WC11 Field and PSR-Derived Soil Moisture Fields Observed in the WC Watershed and the SMEX02 Regional Site in Iowa During SMEX02

Site	Date	Minimum (%v/v)	Maximum (%v/v)	Mean (%v/v)	Median (%v/v)	Variance $(\%v/v)^2$	Skewness	Kurtosis	CV
WC11 Field	26 Jun	5.40	36.70	16.04	14.90	48.66	1.08	0.91	0.44
	27 Jun	5.00	35.50	15.67	14.30	36.46	1.17	1.66	0.39
	28 Jun	6.60	36.10	17.18	17.00	40.05	0.49	−0.04	0.37
	29 Jun	4.33	29.50	13.76	13.45	23.45	0.33	0.17	0.35
	30 Jun	5.07	24.20	13.37	12.10	24.48	0.47	−0.83	0.37
	1 Jul	4.40	22.05	11.84	11.20	15.08	0.35	−0.43	0.33
	3 Jul	0.00	28.55	12.29	12.35	22.00	0.69	1.57	0.38
	5 Jul	17.40	36.90	27.10	27.10	18.85	−0.11	−0.54	0.16
	7 Jul	12.75	39.15	30.07	30.55	21.00	−0.72	1.40	0.15
	8 Jul	16.55	36.15	26.91	26.60	15.66	−0.17	−0.12	0.15
	9 Jul	15.55	33.40	23.29	23.05	19.24	0.25	−0.84	0.19
	10 Jul	27.30	43.17	36.80	36.85	9.98	−0.39	−0.01	0.09
WC Watershed	25 Jun	14.66	25.32	18.37	17.66	8.88	0.41	−1.13	0.16
	27 Jun	13.67	22.19	16.90	16.21	7.26	0.21	−1.61	0.16
	29 Jun	14.43	25.58	18.20	17.43	7.08	0.67	−0.39	0.15
	1 Jul	15.71	27.24	20.07	19.81	6.91	0.53	−0.49	0.13
	4 Jul	17.91	30.68	23.08	22.40	5.87	0.62	0.24	0.10
	8 Jul	16.41	24.87	20.63	20.65	1.73	−0.03	1.23	0.06
	9 Jul	17.58	28.60	23.13	23.04	3.86	0.15	0.48	0.08
	10 Jul	20.78	36.23	27.53	27.20	7.63	0.67	0.92	0.10
	11 Jul	26.16	51.00	35.08	34.60	25.49	0.54	−0.01	0.14
	12 Jul	20.41	33.27	27.72	27.97	8.29	−0.24	−0.37	0.10
SMEX02 Regional Site	25 Jun	8.93	28.29	15.88	15.88	6.40	0.28	0.59	0.16
	27 Jun	8.25	30.12	14.96	14.82	6.91	0.33	0.13	0.18
	29 Jun	7.48	31.63	15.41	15.22	6.46	0.46	1.16	0.16
	1 Jul	6.67	36.26	18.05	18.09	13.31	−0.04	0.33	0.20
	4 Jul	5.00	51.00	19.56	18.72	46.39	1.67	5.12	0.35
	8 Jul	8.68	51.00	22.72	22.41	22.03	0.36	1.27	0.21
	9 Jul	8.85	51.00	20.95	21.11	18.56	0.36	1.71	0.21
	10 Jul	9.81	51.00	28.15	27.33	43.68	0.81	1.34	0.23
	11 Jul	10.51	51.00	31.77	29.84	82.71	0.58	−0.34	0.29
	12 Jul	9.24	51.00	26.81	25.18	64.70	1.14	1.32	0.30

where $s_i(t)$ is the soil moisture observation at location i at time t, j is an index of locations, and m is the total number of observation locations.

[17] In EOF analysis, the PCs and EOFs of a data set are generated by conducting an eigenanalysis of the covariance matrix of the data set. If X denotes an $m \times n$ matrix consisting of the spatial anomalies of a soil moisture data set, where m is the number of sampling locations and n is the sampling days, then the covariance matrix R ($n \times n$) can be written as

$$R = \frac{1}{m} X^T X \tag{6}$$

where superscript T indicates the matrix transpose. The spatial covariance matrix determines the correlation of spatial anomalies between times [*Perry and Niemann*, 2007; *Jawson and Niemann*, 2007].

[18] Next we compute the eigenvectors and eigenvalues of the covariance matrix R, which satisfy the equation

$$RE = LE \tag{7}$$

where E is an $n \times n$ matrix with columns consisting of the eigenvectors of R, and the diagonal matrix L ($n \times n$) contains the corresponding eigenvalues. Each eigenvector represented by the columns of matrix E is a time series and is referred to as 'principal components' or PCs. The related EOF pattern can be obtained by projecting the spatial anomaly matrix X onto the matrix E as

$$F = XE \tag{8}$$

where the columns of matrix F ($m \times n$) contain the EOF patterns. The amount of variance explained by each EOF/PC pair is calculated by dividing the corresponding eigenvalue by the trace of diagonal matrix L [*Jawson and Niemann*, 2007]. The original spatial anomaly data set X can be rebuilt by multiplying the EOF matrix with the transpose of the PC matrix E as

$$X = FE^T \tag{9}$$

[19] This diagonalization of the covariance matrix R in equation (7) causes a rotation of the original coordinate axes in multidimensional space, where each sampling day/time has a dimension. The first/primary axis in the multidimensional space is the direction that explains the maximum covariance in the spatial anomaly data set. The EOF/PC pair along this direction is therefore, referred to as the primary EOF/PC pair. Each new axis is orthogonal to the other axes and explains the most remaining covariance. Thus, the sampling days are replaced by the new axes due to the transformation. The eigenvalues indicate the amount of variance occurring in the direction of each new axis.

Table 2. Parameters and Goodness of Fit of Isotropic Theoretical Models Fitted to Experimental Semivariograms of Theta Probe Measured and PSR-Derived Soil Moisture Fields, Observed During the SMEX02 Campaign in Iowa

Site	Date	Model Type[a]	Nugget C_0	Sill $C_0 + C$	Nugget/Sill $C_0/(C_0+C)$	Model Range[b] (m)	Practical Range[c] (m)	r^2	p value[d]
WC11 Field	26 Jun	S	9.80	48.01	0.204	78	78	0.570	<0.0001(N)
	27 Jun	S	2.10	43.73	0.048	103	103	0.483	<0.0001(N)
	28 Jun	S	14.20	41.64	0.341	146	146	0.726	0.0701[e]
	29 Jun	S	8.07	26.65	0.303	113	113	0.588	0.3864[e]
	30 Jun	S	5.24	29.06	0.180	175	175	0.899	0.0021[f]
	1 Jul	S	8.26	16.53	0.500	230	230	0.706	0.2460[e]
	3 Jul	S	11.80	24.80	0.476	307	307	0.833	0.0167[e]
	5 Jul	S	7.50	20.08	0.374	140	140	0.668	0.6399[e]
	7 Jul	S	6.96	22.23	0.313	115	115	0.459	0.0455[e]
	8 Jul	S	8.80	17.61	0.500	199	199	0.700	0.3276[e]
	9 Jul	S	8.24	21.05	0.391	173	173	0.799	0.0535[e]
	10 Jul	S	4.86	10.41	0.467	101	101	0.387	0.4107[e]
WC Watershed	25 Jun	G	0.01	19.61	0.001	9855	>6670	0.999	<0.0001(N)
	27 Jun	G	0.12	16.86	0.007	11882	>6670	0.999	<0.0001(N)
	29 Jun	G	0.09	13.83	0.007	8556	>6670	0.999	<0.0001(N)
	1 Jul	G	0.04	12.37	0.003	7361	>6670	0.996	0.0019[f]
	4 Jul	G	0.36	8.98	0.040	6305	6305	0.999	0.0231[e]
	8 Jul	G	0.00	2.07	0.000	2581	2581	0.510	0.4941[e]
	9 Jul	G	0.22	4.66	0.047	3724	3724	0.985	0.9093[e]
	10 Jul	G	0.01	6.97	0.001	2893	2893	0.675	0.0348[e]
	11 Jul	G	0.62	4.40	0.141	2044	2044	0.252	0.0498[e]
	12 Jul	G	0.01	7.65	0.001	2944	2944	0.951	0.2763[e]
SMEX02 Regional Site	25 Jun	E	0.66	6.83	0.097	42000	42000	0.973	0.0100[e]
	27 Jun	E	0.01	7.45	0.001	24900	24900	0.934	0.0100[e]
	29 Jun	E	0.01	6.96	0.001	21900	21900	0.982	0.0100[e]
	1 Jul	E	1.53	18.17	0.084	63300	>52150	0.992	0.0100[e]
	4 Jul	E	1.80	52.13	0.035	56700	>52150	0.978	0.0100[e]
	8 Jul	E	0.01	23.35	0.000	21900	21900	0.980	0.0100[e]
	9 Jul	E	0.01	18.82	0.001	19500	19500	0.990	0.0100[e]
	10 Jul	E	4.70	44.99	0.104	38400	38400	0.950	0.0100[e]
	11 Jul	E	12.40	133.00	0.093	118500	>52150	0.987	0.0100[e]
	12 Jul	E	8.10	97.20	0.083	102300	>52150	0.981	0.0100[e]

[a]G, Gaussian; E, exponential; S, spherical.
[b]Range for Gaussian model is $\approx 3^{0.5}A_0$, for exponential model is $3A_0$, and for spherical model is A_0.
[c]Practical range indicates the actual correlation length.
[d]N, Soil moisture distribution not normal.
[e]Soil moisture distribution normal at the 0.01 significance level.
[f]Soil moisture distribution normal at the 0.001 significance level.

[20] In this study, we have 12 days of theta probe measurements for the WC11 field, and 10 days of PSR-derived soil moisture observations for the WC watershed and the SMEX02 regional site. Therefore, the total number of EOF/PC patterns generated from the spatial anomaly data set is also 12 in case of WC11 field, and 10 each for the watershed and the regional domain. Furthermore, to explore the relationship between the spatial variability of soil moisture and various regional characteristics, a simple correlation analysis was conducted at the watershed and regional scales using the normalized values of all the variables involved in the analysis.

4. Results and Discussions

4.1. Variogram Analysis

[21] Table 1 presents the summary statistics of the theta probe based measurements in the WC11 field, and PSR-derived soil moisture at the watershed and regional scales obtained during the SMEX02 campaign. Within a span of 12 days (from 26 June to 10 July 2002) during which the observations were taken, the mean soil moisture content in the WC11 field varied from a minimum value of 11.84 (%v/v) on 1 July to a maximum value of 36.80 (%v/v) on 10 July. In the WC watershed, the mean soil moisture varied within a range of 16.90 (%v/v) to 35.08 (%v/v) for a period of 10 days from 25 June to 12 July 2002. The eleventh of July was the wettest day with the highest mean, whereas 27 June was the driest day with the lowest mean soil moisture content in the watershed. At the regional scale, the mean soil moisture content showed a minimum value of 14.96 (%v/v) on 27 June and a maximum of 31.77 (%v/v) on 11 July 2002. The statistics provide how the mean, standard deviation, variance, skewness, kurtosis, and the coefficient of variation (CV) vary at different spatial scales during SMEX02 in Iowa.

[22] Before conducting the geostatistical analysis, a normality test (based on the sample size, n: Shapiro-Wilk test ($n < 2000$) for the WC11 field and the WC watershed; and Kolmogorov-Smirnov-Lilliefers (KSL) test ($n > 2000$) for the SMEX02 regional domain) was performed using a statistical analysis software, JMP (SAS Institute Inc., Cary, North Carolina) to check whether the soil moisture values at the considered spatial scales were distributed normally. The Q-Q plots as well as the p values for the normality test (see Table 2) proved that the soil moisture data have a fairly normal distribution at $\alpha = 0.01$ significance level. At the field and the watershed scales, we have a few exceptions,

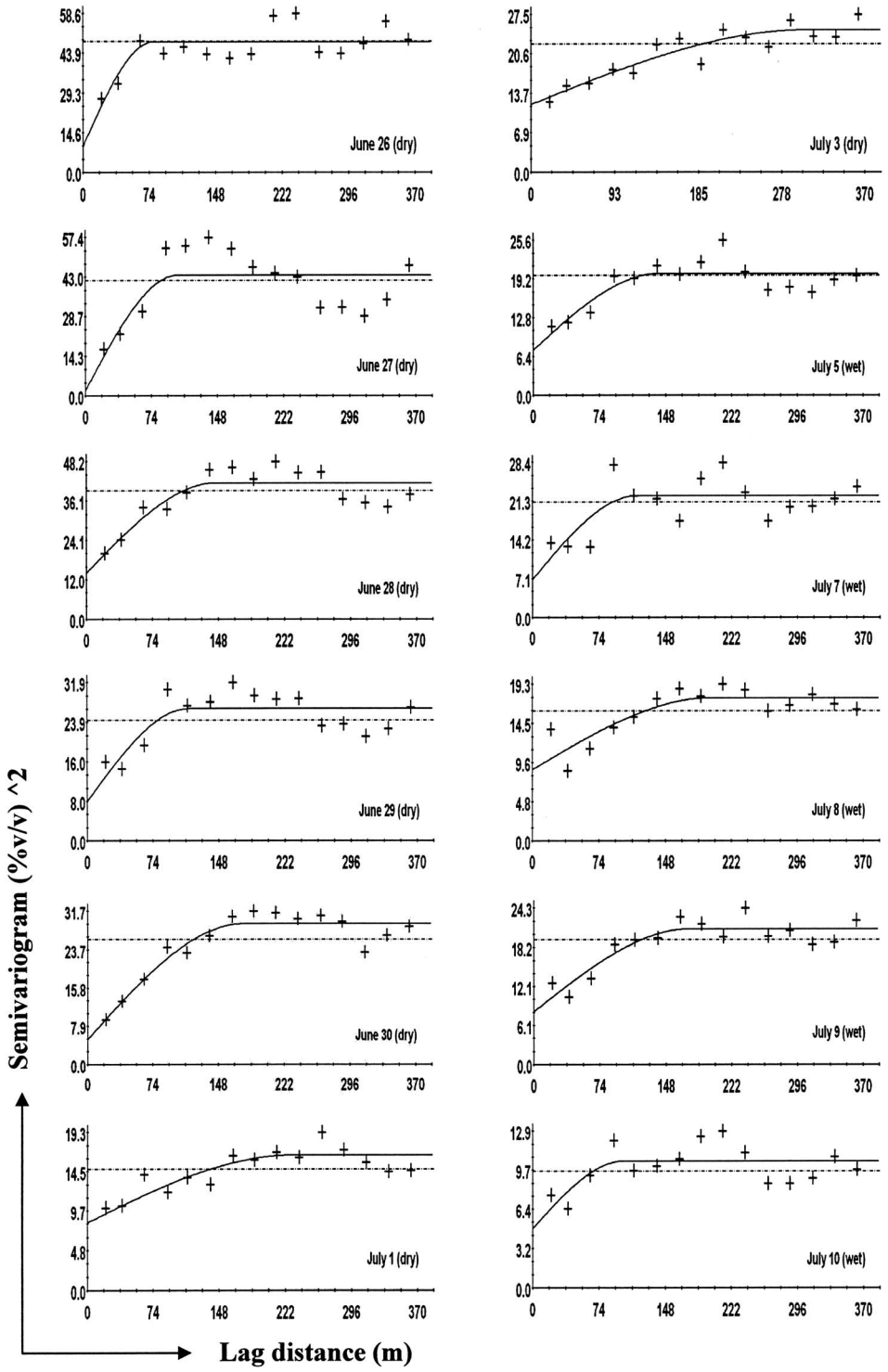

Figure 4. Theoretical semivariograms (solid lines) fitted to the isotropic experimental semivariograms (+) of the theta probe measured soil moisture data within the WC11 field (Iowa), during SMEX02.

but for analyses purposes, the data distribution was considered normal.

[23] Table 2 gives a summary of the parameters and goodness of fit of the isotropic theoretical models fitted to the experimental semivariograms of the theta probe measured and PSR-derived soil moisture data set at different scales during SMEX02. For estimating the semivariograms in the WC11 field, the lag distances were grouped with fairly large number of data pairs (i.e., 21 m, 64; 39 m, 127; 64 m, 125; 90 m, 236; 113 m, 241; 138 m, 248; 164 m, 204; 188 m, 229; 213 m, 216; 238 m, 229; 263 m, 346; 288 m, 295; 313 m, 218; 338 m, 230; and 363 m, 207). At the field scale, an isotropic spherical model with a nugget provides a reasonably good fit to the daily soil moisture semivariograms with the correlation lengths varying between 78 m and 307 m. For estimating the semivariograms within the

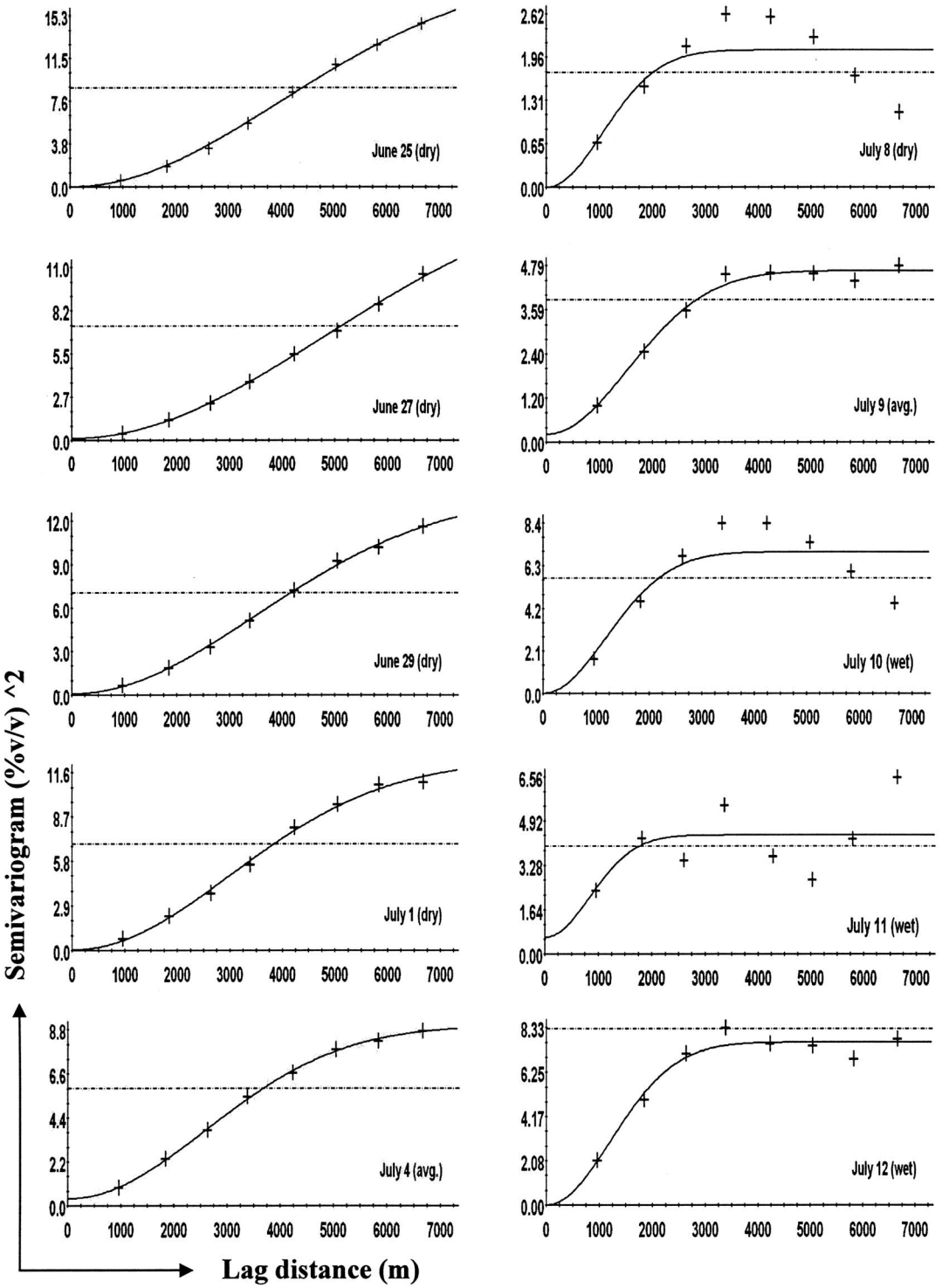

Figure 5. Theoretical semivariograms (solid lines) fitted to the isotropic experimental semivariograms (+) of the PSR based soil moisture fields within the WC watershed (Iowa), during SMEX02.

WC watershed, the lag distances were grouped with reasonably large number of data pairs (i.e., 960 m, 262; 1842 m, 403; 2631 m, 386; 3381 m, 347; 4231 m, 406; 5045 m, 277; 5835 m, 270; and 6670 m, 250). Similarly, for the SMEX02 regional site, lag distances ranging between 2513 m and 52,150 m were grouped with large number of data pairs for generating the semivariograms (i.e., 2513 m, 264,232; 5595 m, 658,734; 9085 m, 1,120,473; 12,633 m, 1,355,262; 16,216 m, 1,735,274; 19,834 m, 1,849,222; 23,418 m, 2,070,160; 30,587 m, 2,270,976; 34,203 m, 2,139,316; 37,781 m, 2,192,217; 41,371 m, 2,029,154; 44,941 m, 1,968,104; 48,540 m, 1,777,658; and 52,150 m, 1,627,827). At the watershed scale, an isotropic Gaussian model with a nugget provides a good fit to the daily soil moisture semivariograms with the correlation lengths varying between 2044 m and 11,882 m. Here, the modeled spatial correlation

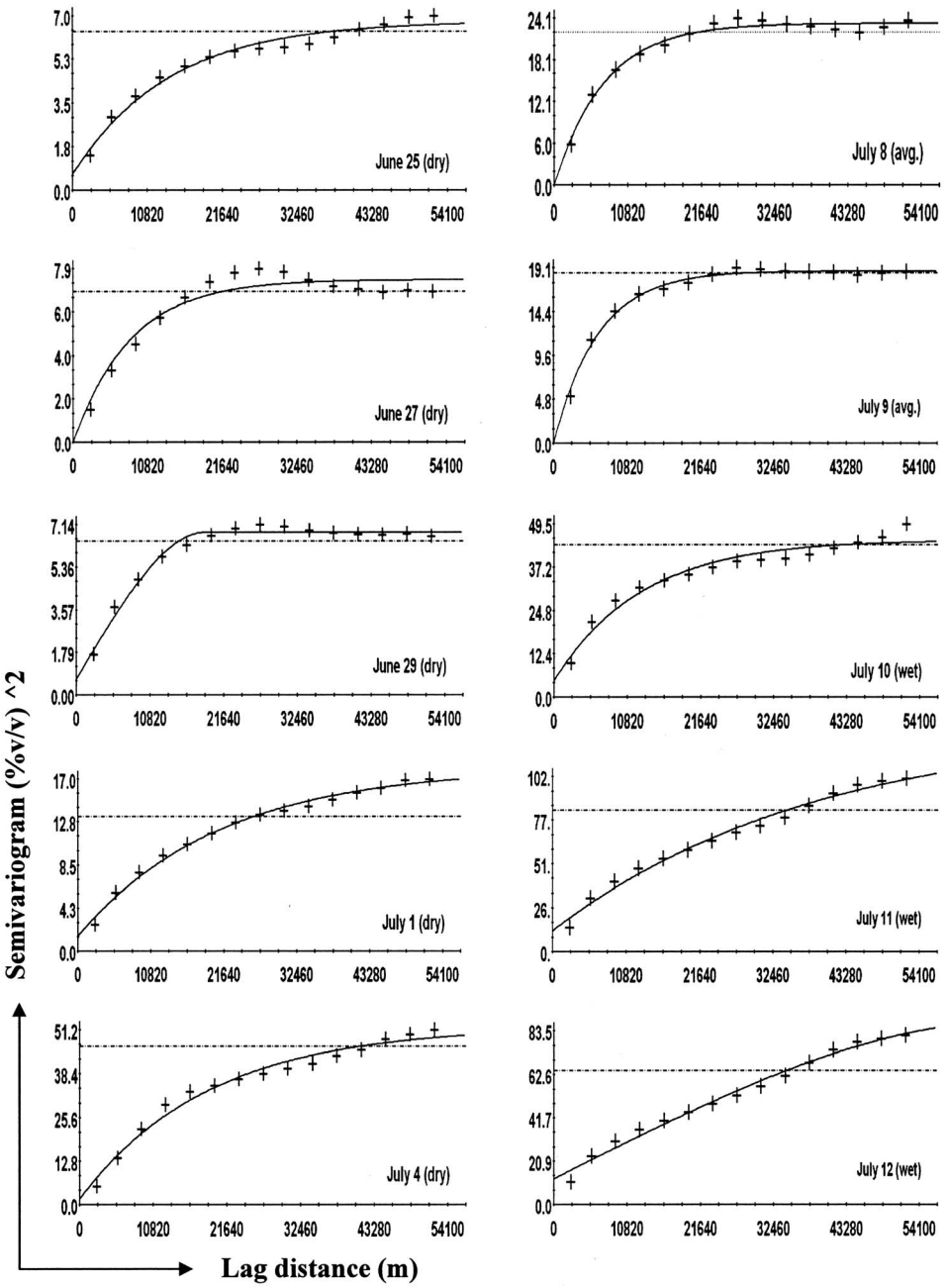

Figure 6. Theoretical semivariograms (solid lines) fitted to the isotropic experimental semivariograms (+) of the PSR based soil moisture fields within the SMEX02 regional site (Iowa), during the SMEX02 campaign.

length (e.g., 11,882 m) larger than the maximum lag distance (~6670 m at the watershed scale) used in estimating experimental semivariograms implies that the soil moisture field was extrapolated for the purpose of model fitting. In other words, soil moisture is correlated for the entire lag distance used in experimental semivariogram estimation on such occasions. On the other hand, at the regional scale, the exponential model with a nugget provides a reasonably good fit for the experimental semivariograms with the correlation lengths ranging between 19,500 m and 118,500 m.

[24] Table 2 shows that the nugget value is higher at the field scale for the theta probe soil moisture measurements. The nugget variance is low at the watershed scale, but increases as it goes toward the regional scale for the PSR-derived soil moisture fields (see Table 2). The nugget represents the measurement errors and any microheterogeneity present in soil moisture. In case of the remotely sensed PSR data, the nugget may also represent the level of image smoothing used in the soil moisture retrieval algorithm to obtain the soil moisture estimates. At the field scale, the microheterogeneity of (point scale) soil moisture is higher resulting in larger values of the nugget for the WC11 field. On the other hand, at the watershed and regional scales, the subpixel soil moisture variability smoothens out during the soil moisture retrieval process lowering the nugget

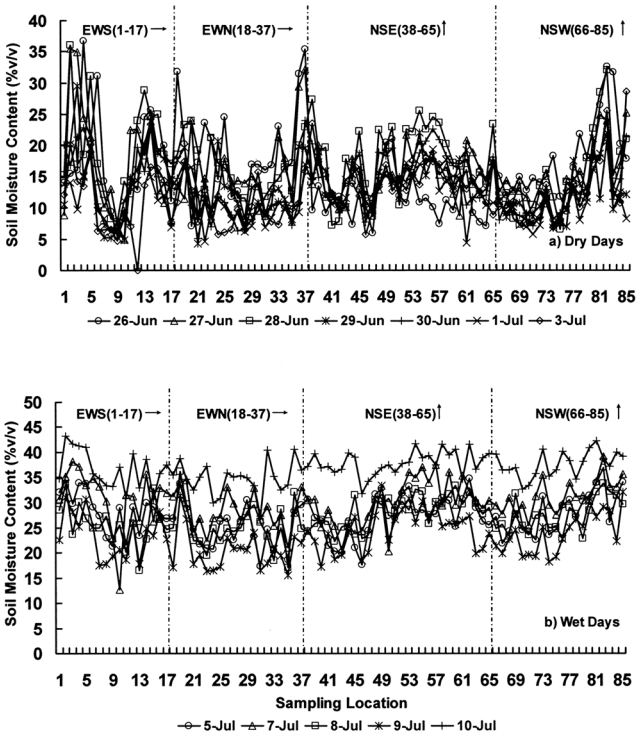

Figure 7. Signature of theta probe soil moisture measurements along the four transects (EWS, EWN, NSE, and NSW) in the WC11 field on (a) dry and (b) wet days during SMEX02.

variance. In addition, the measurement/calibration errors of PSR based soil moisture (at the measurement support scale) under a variety of land surface features may also have contributed toward the nugget variance. Therefore, as we increase the sampling extent, from the watershed scale to the regional scale, the measurement errors get lumped leading to increased values of the nugget for the semivariograms generated from the PSR data set.

[25] At the field scale, for the theta probe soil moisture data collected from the WC11 field, we observe that the correlation lengths are usually higher for relatively dry days with the exception of 26 June 2002 (Table 2). The correlation lengths are comparatively lower on the days when the soil is wetter. The correlation lengths vary between 101 m and 199 m for the wet days as against between 78 m and 307 m for the dry days. Among the wet days, the correlation length is the lowest on 10 July when the soil moisture content is the highest due to the precipitation event (CV = 0.09). This does not match with the findings of *Mohanty et al.* [2000] for the LW21 field, where the correlation length on 11 July 1997 (CV = 0.23), after the precipitation event on 10 July, was 348 m (lowest correlation length being <100 m). LW21 is a silt loam field with flat topography [*Mohanty and Skaggs*, 2001], while the WC11 field has soil texture with a higher silt content (~47%) with topography consisting of hilltop and slope [*Jacobs et al.*, 2004]. The topography of the WC11 field may be responsible for the lateral drainage following the rainfall event, resulting in lower correlation length on the wettest day. The variation in the correlation length with changes in soil moisture conditions within the WC11 field is shown in Figure 4.

[26] Similar to the field-scale observations, at the watershed scale the correlation lengths are higher on dry days (2581–11,882 m) compared to relatively wet days (2044–2944 m) (see Table 2). Thus, with the increase in wetness, the correlation length decreases within the watershed. Figure 5 shows how the correlation length increases with decreasing mean soil moisture content within the watershed. As compared to the watershed scale, at the regional scale, we observe an opposite trend with correlation length being higher on wet days compared to the dry days (see Table 2 and Figure 6). The correlation length values ranged between 38,400 m and 118,500 m on wet days as opposed to between 24,900 m and 63,300 m on dry days. The only exception is 1 July 2002 when the correlation length (63,300 m) is a bit higher compared to the other dry days. Thus, the increase in moisture content seems to have an opposite impact on the spatial correlation length at the regional scale as opposed to the field and watershed scales. The precipitation map (Figure 3b) shows that the SMEX02 regional site received medium to high rainfall throughout on 10 July 2002. Consequently, the soil moisture correlation length on 11 July was highest as the study area was closer to saturation on account of the rainfall event on the previous day. But similar observations were not made after the precipitation event on 10 July within the WC11 field or the WC watershed. Thus, apart from precipitation, other geophysical factors seem to dominate the variability and spatial structure of soil moisture at the field and watershed scales.

[27] At the field scale, the fitted isotropic variograms reached their sill fairly well on almost all the days the theta probe measurements were taken. But at the watershed and regional scales, the variograms did not reach their sills on most of the days exhibiting nonstationarity in the data set. This nonstationarity in the soil moisture data may be due to the various geophysical factors (e.g., topography, soil texture, vegetation, etc.) that impact the soil moisture variability. It may also be due to the measurement errors or the calibration issues related to the PSR-derived soil moisture fields at the watershed and the regional scales. We have not investigated the issue of nonstationarity in detail in this paper, as we are more interested in finding the various geophysical factors controlling the spatiotemporal variability of soil moisture at different scales in an agricultural landscape employing the data collected by two different platforms: ground-based theta probe measurements and the PSR-derived airborne RS data. Therefore, this matter requires a more detailed investigation and is beyond the scope of this paper.

4.2. EOF Analysis

4.2.1. Field Scale

[28] Figure 7 shows the signature of the 12 day long theta probe soil moisture contents measured along the four transects (see Figure 1) in the WC11 field during SMEX02. For EOF analysis, only 85 (of a total of 92) locations were selected where the soil moisture contents were recorded every day for the 12 day period. Transects EWN and EWS oriented east–west contain 20 and 17 sampling locations (marked in +ve x direction), respectively. Transects NSE and NSW in the north–south direction contain 28 and 20 sampling locations (marked in the +ve y direction), respectively. Twelve EOF/PC pairs were generated from the

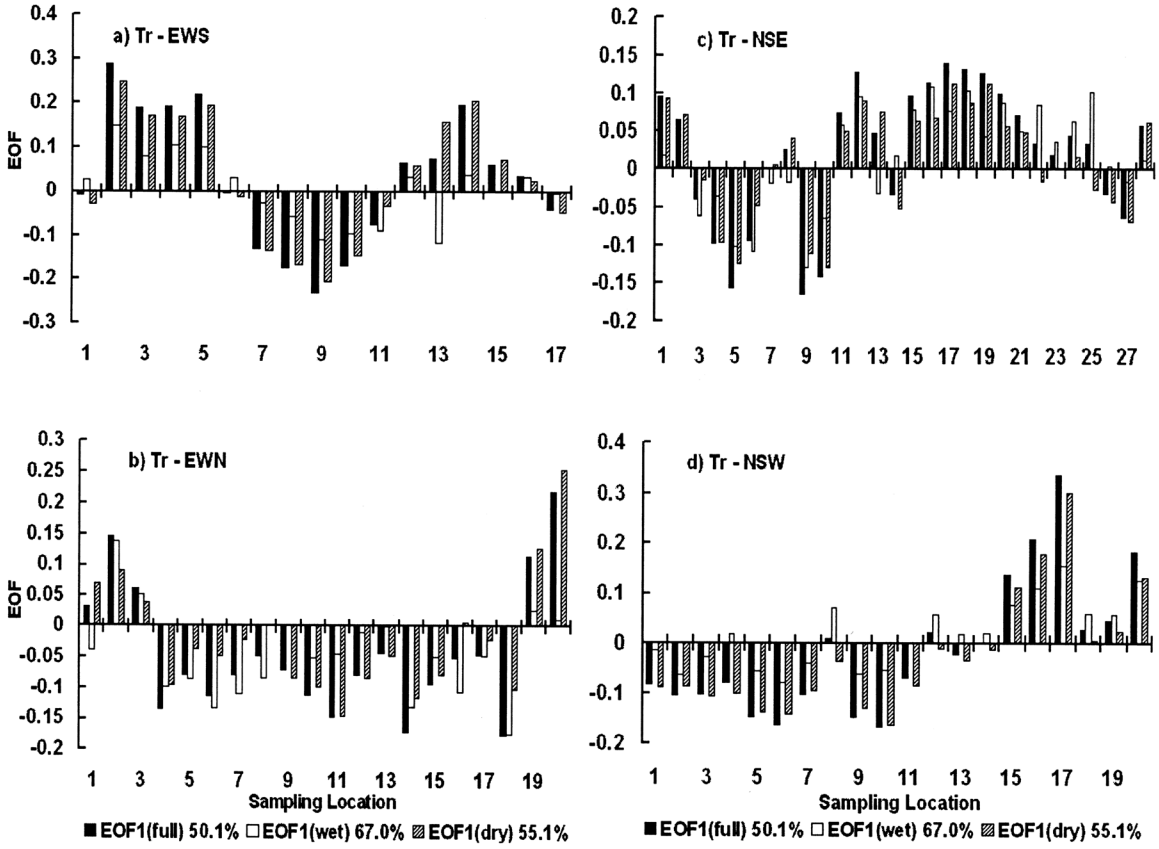

Figure 8. The primary EOFs (and the variance explained by them) for the theta probe soil moisture measurements along the four transects (EWS, EWN, NSE, and NSW) in the WC11 field (for the complete data set, wet days, and dry days) during SMEX02.

EOF analysis of the complete soil moisture data set for the WC11 field. The first EOF (also, known as the primary EOF) values are plotted transect-wise in Figures 8a–8d, for the four transects in the field. The eigenvalues associated with the EOF/PC pairs can be used to determine the amount of variance explained by each EOF/PC pair. Figure 9a shows the scree plot of the percent variability explained by each EOF/PC pair at the field scale. The first four EOFs together explain about 81% of the total variability, whereas the first three EOFs explain approximately 74% of the total variance. The primary EOF (or EOF1) explains about 50% of the total soil moisture variance. The rest of the EOFs after the fourth one each explain less than 5% of the total variability. Additional analysis from the WC12 field (results not presented here) also showed that the first four EOFs explained 83% of the variance, while the first three of the EOF patterns explained nearly 73% of the total variability. Further, the primary EOF explained only 36% of the total variance in the WC12 field. Therefore, at the field scale, we observe that the soil moisture patterns obtained for the 12 day period can largely be explained by only four underlying spatial structures or EOF patterns that in turn may be correlated to the various geophysical characteristics, such as, soil texture, topography, land use/land cover, etc.

[29] Figure 10a shows the weighted PC series obtained from the EOF analysis of the 12 day soil moisture anomalies for the WC11 field. The weighted PCs are obtained by multiplying the PCs by the amount of variance explained by them. Thus, the weighted PCs give a measure of the relative importance of the EOFs in describing the variance in daily soil moisture pattern. Further, the weighted PCs exhibit temporal variations which can be associated with the occurrence of rainfall events and the following dry down periods [*Jawson and Niemann*, 2007]. It is evident from Figure 10a that the primary EOF is dominant throughout the observation period during the SMEX02 campaign.

[30] Different geophysical processes are significant in the vadose zone water balance depending on the overall soil moisture content which in turn could lead to stronger relationships between the soil moisture patterns and certain regional characteristics for wet or dry days [*Jawson and Niemann*, 2007]. To examine this possibility, the soil moisture data set was divided into wet, average, and dry days within the WC11 field (Figure 11a) as per the ±25% standard deviation rule proposed by *Jawson and Niemann* [2007]. Further, the EOF analysis was individually conducted using the spatial soil moisture anomalies obtained for the wet, average, and dry days. At the field scale, the primary EOF explains about 67% of the total amount of variance on wet days, while on the dry days, it explains about 55% of the total soil moisture variability. The amount of the total variance explained as well as the distribution of the primary EOF values at most of the sampling locations for the dry days is very similar to those generated from the complete soil moisture data set (see Figures 8a–8d). Note that the area experienced a rainfall event on 10 July 2002. This similarity between the primary EOFs of the dry days and the complete data set implies that the primary EOF (or

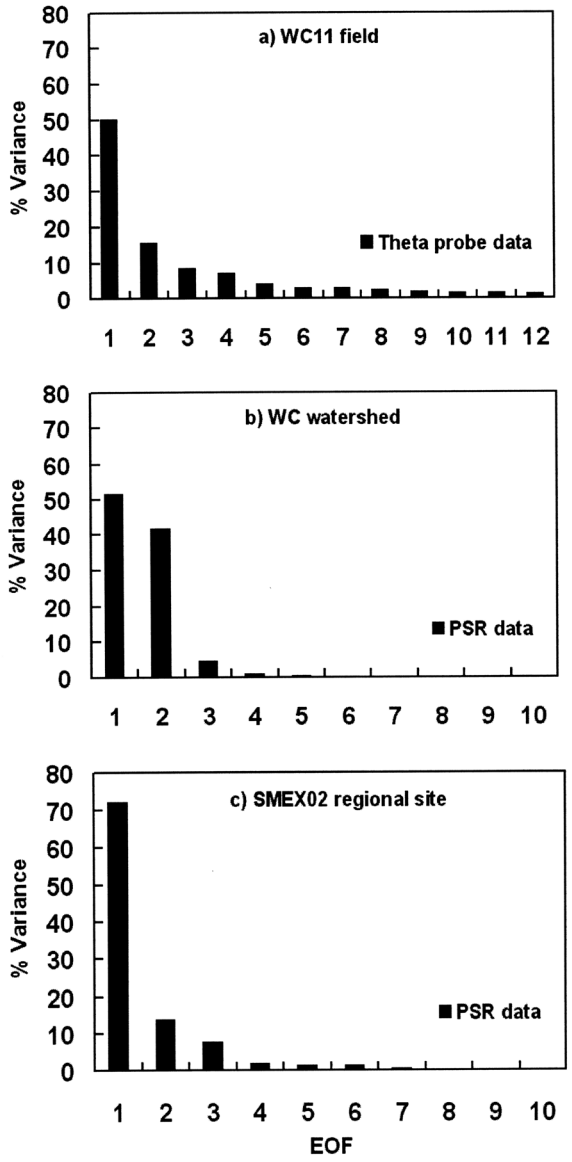

Figure 9. Scree plot of the percent variability explained by each EOF (from complete data set) in (a) the WC11 field, (b) the WC watershed, and (c) the SMEX02 regional site, during the SMEX02 campaign.

EOF1) of soil moisture at the field scale, is mainly dominated by the mean soil moisture status of the field during the entire duration of the SMEX02 campaign rather than solely by precipitation. The fact that the primary EOF of wet days explains just 67% of the variance (compared to 55% and 50% for the dry days and the complete data set, respectively) further strengthens this inference.

4.2.2. Watershed Scale

[31] The PSR based soil moisture evolution map for the WC watershed during the SMEX02 campaign is shown in Figure 12. The EOF analysis of the complete 10 day soil moisture data set for the watershed generated ten EOF/PC pairs. Figure 13a shows the first three EOF patterns obtained from the analysis. From the scree plot shown in Figure 9b, it is apparent that the first two EOFs together explain more than 93% of the total variance. The rest of the eight EOFs each explain less than 5% of the total variance. In fact, from the 5th EOF onward, the variance explained by the EOF patterns is almost negligible. The primary EOF explains 51.5%, while the second EOF (EOF2) explains about 42% of the total variance. Therefore, the soil moisture patterns within the WC watershed obtained for the 10 day period can largely be explained by only two underlying spatial structures. Figure 3a shows that the watershed received a high rainfall on 10 July 2002 and the distribution of precipitation was relatively uniform. The soil moisture pattern on 11 July shows above average soil moisture content in northwestern and southeastern part of the watershed (Figure 12). A close examination of the EOF patterns in Figure 13a reveals that the EOF1 and EOF2 have high values in the southeastern

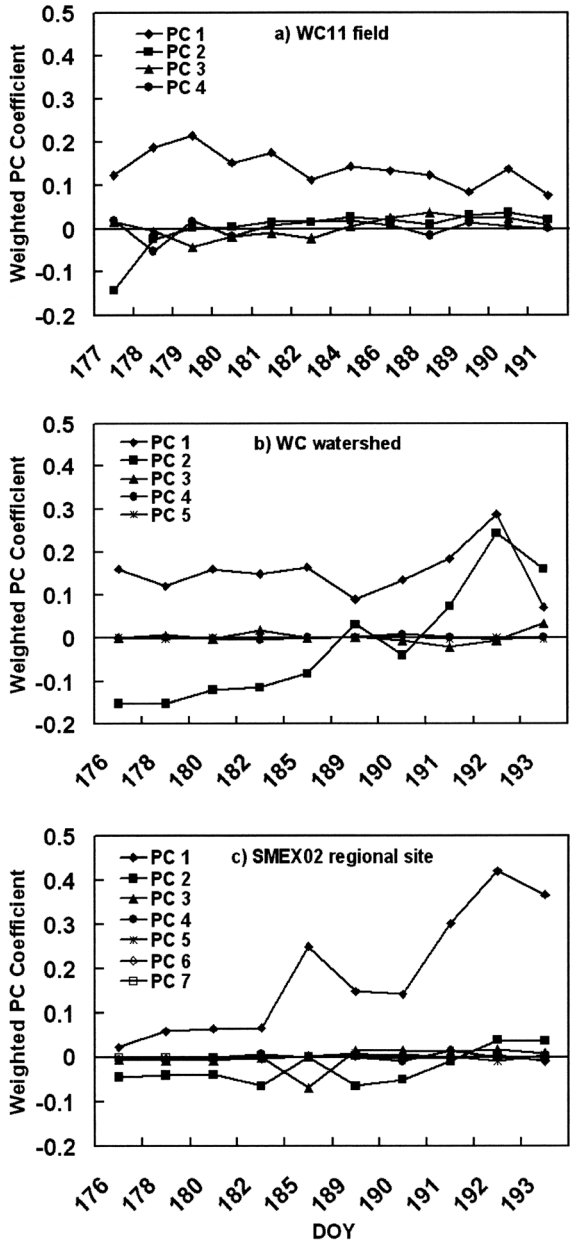

Figure 10. Weighted coefficient time series of EOFs generated from theta probe soil moisture measurements in (a) the WC11 field and PSR-derived soil moisture in (b) the WC watershed and (c) the SMEX02 regional site, during the SMEX02 campaign.

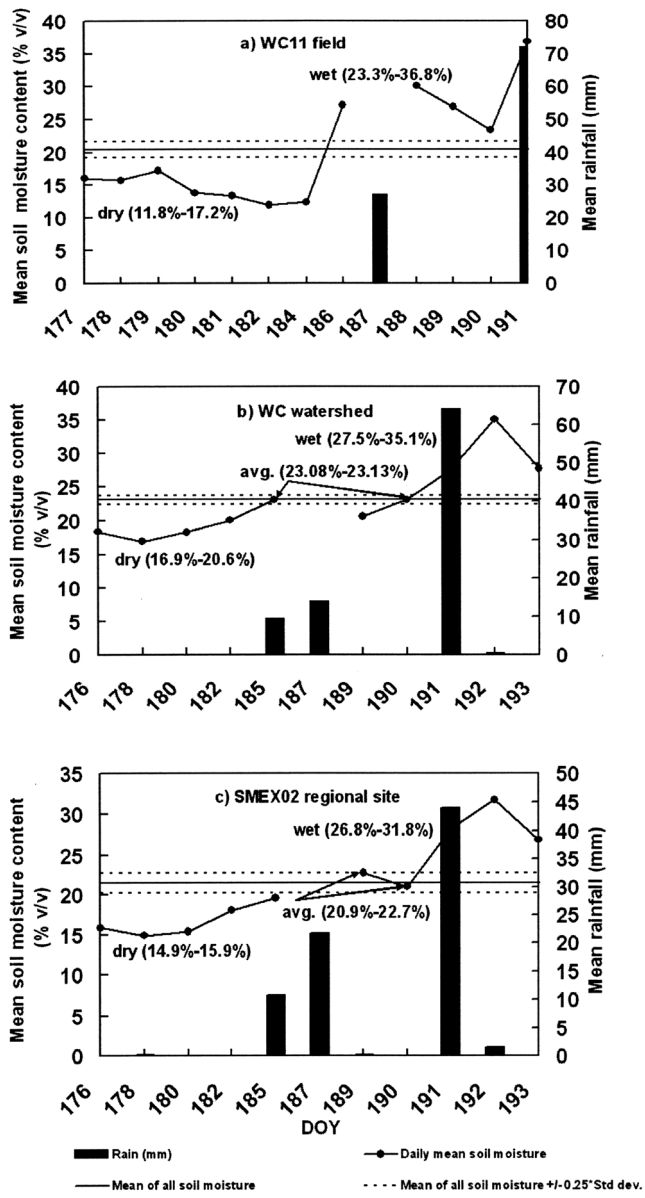

Figure 11. Daily mean soil moisture and the classification of days as wet, average, and dry days within (a) the WC11 field, (b) the WC watershed, and (c) the SMEX02 regional site, during the SMEX02 campaign.

and northwestern part of the watershed, respectively. From the weighted PC series (Figure 10b), it is obvious that the effect of primary EOF (EOF1) is dominant throughout the observation period, except for the last day when EOF2 is more dominant. The influence of both EOF1 and EOF2 rises sharply after the 10 July rainfall event.

[32] Figure 11b shows the classification of the PSR-derived soil moisture data into wet, average or dry days within the WC watershed. At the watershed scale, the primary EOF itself explains more than 90% of the total amount of variance for both the average and dry days, while for the wet days, it explains about 87% of the variance (Figure 13b). The primary EOF for the wet days has high values in the northwestern and southeastern parts within the watershed. This EOF pattern is similar to the soil moisture pattern on 11 July 2002 (Figure 12), where the above average soil moisture values are also clustered in the northwestern and southeastern parts of the watershed. Note that the watershed received a rainfall event on the previous day on 10 July 2002 (Figure 3a). The primary EOF pattern for the dry days (Figure 13b) is similar to the primary EOF pattern obtained for the complete soil moisture data set for the 10 day period (Figure 13a). Based on these observations, we infer that within the WC watershed, the primary EOF is not affected solely by precipitation but seems to be controlled by other geophysical parameters (e.g., soil texture, topography) as well. This observation will be examined later on in the study by performing the correlation analysis.

4.2.3. Regional Scale

[33] Figure 14 shows the PSR-derived soil moisture evolution map for the SMEX02 regional study site in Iowa.

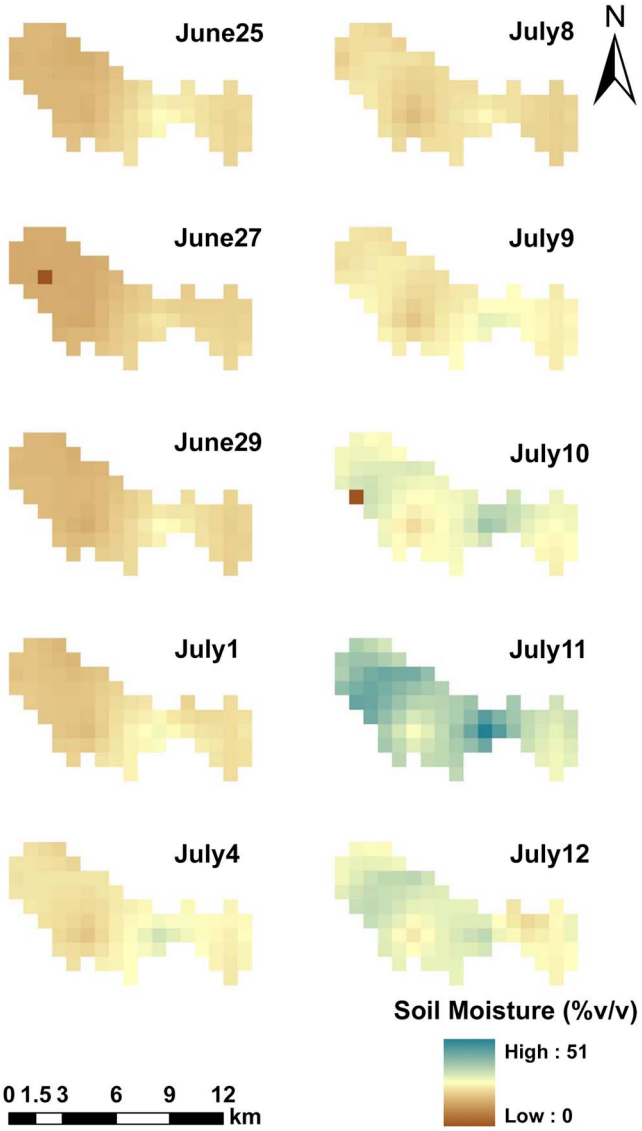

Figure 12. Soil moisture evolution map estimated from PSR remote sensing data within the WC watershed (Iowa), during the SMEX02 campaign.

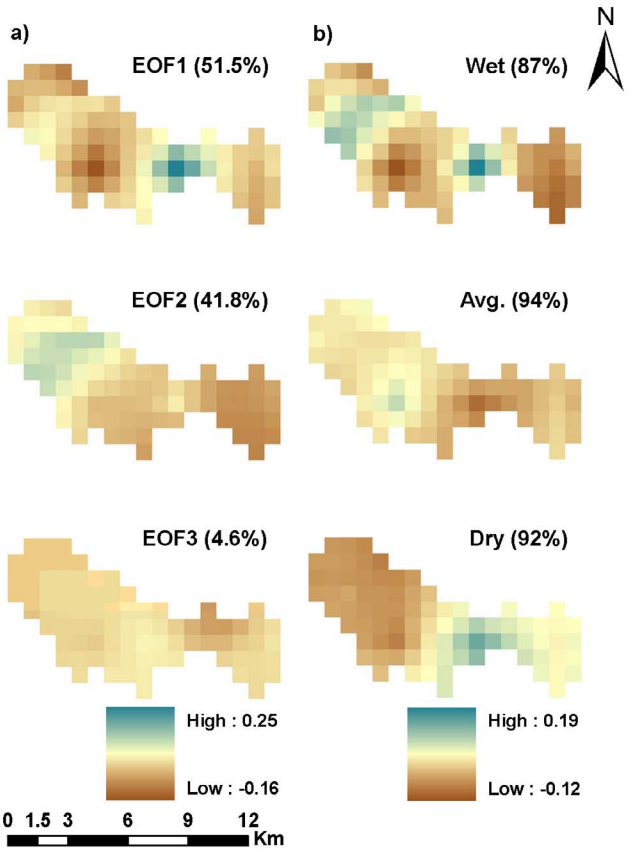

Figure 13. (a) The first three EOFs generated from the spatial anomalies of PSR-derived soil moisture and the variance explained by each EOF/PC pair. (b) The primary EOFs obtained from wet, average and dry days at the WC watershed during SMEX02.

Three of the ten EOF/PC pairs generated from the EOF analysis for the study area are shown in Figure 15a. The scree plot of the percent variability explained by each EOF pattern at the regional scale during SMEX02 is shown in Figure 9c. From Figure 15a, we observe that the first three EOFs together explain about 93% of the total variance, whereas the first two EOFs together explain nearly 86% of the total variability. Also, at the regional scale, the primary EOF pattern explains more than 70% of the total variance compared to the 50% variance explained by EOF1 at both the field and watershed scales. Thus, the soil moisture patterns obtained for the 10 day period at the regional scale can largely be explained by only three underlying spatial structures. The precipitation map given in Figure 3b shows that the regional site received medium to high rainfall throughout on 10 July 2002, while the precipitation events on 4 and 6 July had localized medium to high rainfall values. The primary EOF pattern (Figure 15a) has high values clustered in the northwest region of the study site which is similar to the above average soil moisture values in the northwestern region of the soil moisture patterns from 10 to 12 July 2002 (Figure 14). Similar to the field and watershed scales, at the regional scale, the primary EOF (EOF1) is dominant throughout the observation period (Figure 10c). The influence of EOF1 rises sharply after each precipitation event and wanes during the dry down periods.

[34] The PSR soil moisture observations for the SMEX02 regional site was classified into wet, average or dry days as shown in Figure 11c. At the regional scale, EOF1 explains more than 90% of the total amount of variance for both the wet and average days, while for the dry days; only 68% of the variance is explained by the primary EOF (Figure 15b). The average days received a moderate rainfall on 6 July, while the wet days experienced a heavy precipitation event on 10 July 2002. The primary EOF pattern for the wet days is similar to the primary EOF pattern obtained for the complete soil moisture data set for the 10 day period as well as the soil moisture patterns from the wet days, i.e., 10–12 July 2002 (see Figures 14, 15a, and 15b). Thus, the primary EOF on average and wet days seems to be related to a combination of regional characteristics, including precipitation. Correlation analysis will help investigate the effect of the various geophysical factors on the spatial EOF structures.

4.2.4. Correlation Analysis

[35] Now that we have decomposed the soil moisture patterns into a small number of orthogonal spatial patterns that together explain a large portion of the total soil moisture variability, we further try to investigate the relationship between these underlying patterns and the regional characteristics that might influence soil moisture. For this, we conducted a correlation analysis between the EOFs and several regional attributes such as; DEM, slope, percent sand, percent clay, VWC and NDVI (Figure 2) at both the watershed and regional scales. All data have been normalized using the respective mean and standard deviation for the correlation analysis, results of which are given in Table 3. To examine the effect of precipitation, we performed the EOF analysis using the NEXRAD precipitation data (Figure 3) and correlated the primary EOF (EOF1) of rainfall with the EOF patterns generated from the PSR soil moisture estimates. At the watershed scale, EOF1 obtained from rainfall data explained 97% of the variability, whereas at the regional scale, it explained about 88% of the total variance. At the watershed scale, the primary EOF (EOF1) of soil moisture is moderately correlated with percent clay and rainfall. This shows that some of the variability of the EOF1 pattern is related to both rainfall and soil texture. The secondary EOF (EOF2) shows a strong correlation with elevation, followed by rainfall, percent clay, percent sand, and slope, while with VWC it has a moderate correlation. Correlation results for the wet, average, and dry days show that the primary EOF of average and dry days has strong correlations with elevation, rainfall, percent sand, and percent clay, whereas with slope and VWC, the correlation is moderate. The primary EOF for the wet days has moderate correlation with all the six geophysical parameters (i.e., elevation, slope, rainfall, percent sand, percent clay, and VWC). Based on these findings, we suggest that the soil moisture variability within the watershed is jointly controlled by topography, rainfall, and soil texture, and to a limited extent by the vegetation parameters.

[36] At the regional scale, Table 3 shows that EOF1 of soil moisture is moderately correlated with elevation, slope, percent sand, but has a higher correlation with percent clay. This implies that some of the variability of the EOF1 pattern is related to both topography and soil texture. EOF2 shows a moderate correlation with rainfall, elevation, and soil texture. The primary EOF of both average and dry days

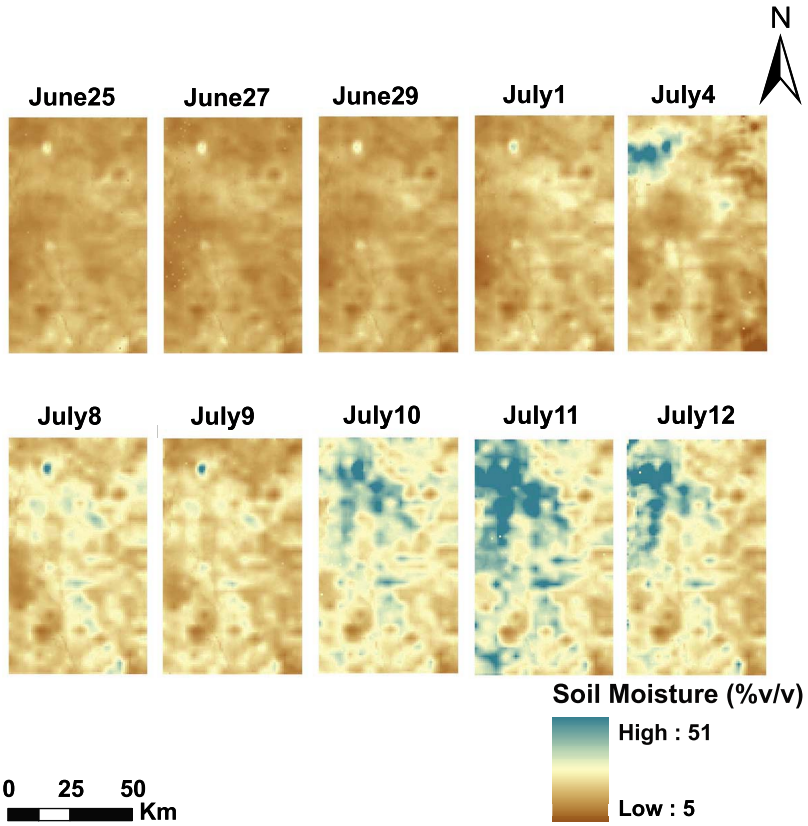

Figure 14. Soil moisture evolution map estimated from PSR remote sensing data within the SMEX02 regional site in Iowa.

is moderately correlated with slope (and/or elevation), soil texture, and rainfall. The primary EOF for the wet days also has a moderate correlation with topography (elevation and slope) and soil texture (percent sand and percent clay), though the correlation is better compared to the average and dry days. However, with rainfall, the correlation is poor. With vegetation parameters (VWC and/or NDVI), all the EOFs for the complete data set as well as the primary EOF of wet, average, and dry days have a poor correlation. The correlation analysis results at the regional scale are comparable to those at the watershed scale. We infer that some of the variability of the EOF patterns is related to topography, soil texture, and rainfall at both the watershed and regional scales. The effect of rainfall on the soil moisture variability is greater at the watershed scale compared to the regional scale. On the other hand, results generally reflect a low correlation at the watershed scale (with few exceptions), and a poor correlation at the regional scale, with respect to the vegetation parameters (VWC, NDVI).

[37] Thus, geostatistics and EOF approach can be used jointly to examine the evolution of the spatiotemporal variability of near-surface soil moisture measured at different support with varying spatial extents. Geostatistics enables us to determine the spatial correlation structure of the soil moisture content under different moisture conditions (i.e., wet, average, and dry days). The spatial correlation lengths obtained can be effectively used for kriging purposes to get an interpolated soil moisture map of the entire study area encompassing the unsampled locations as well. The behavior of the fitted theoretical semivariogram model (especially near the origin and sill) not only gives us an idea about the changing correlation structure of soil moisture during the wetting/drying sequence, but also allows us to speculate the individual or combined effects of various physical controls (e.g., precipitation, topography, soil texture, and vegetation parameters) on soil moisture variability. For example, *Ryu and Famiglietti* [2006] observed two different correlation lengths in their study using the SGP97 ESTAR data in a 50 km × 250 km region. Based on their analysis, they concluded that the smaller-scale correlation (10 ~ 30 km) is governed by soil texture and vegetation, and the larger-scale correlation (60 ~ ≥100 km) by precipitation. In another study using 30 cm deep TDR moisture readings, *Western et al.* [1998] noticed the effects of topography on seasonal evolution of soil moisture with lower correlation lengths during wet winter and longer correlation lengths during dry summer periods in the Tarrawarra catchment, Australia. In our case, based on the geostatistical results, we speculated that other geophysical parameters are also responsible in controlling the soil moisture variability at different spatial scales (field, watershed, and regional scales) in addition to precipitation.

[38] Once, we get a fair/rough idea about the correlation structure and the effects of the physical controls on soil moisture variability, we can employ the EOF technique to breakdown a more dynamic time series of soil moisture in to a lesser number of orthogonal spatial EOF patterns (that are invariant in time) and the corresponding PC components (that are invariant in space). This greatly simplifies our task as we have to deal with only a few spatial EOF structures instead of the whole data set. Usually, the higher-order EOFs are discarded depending on the amount of the total

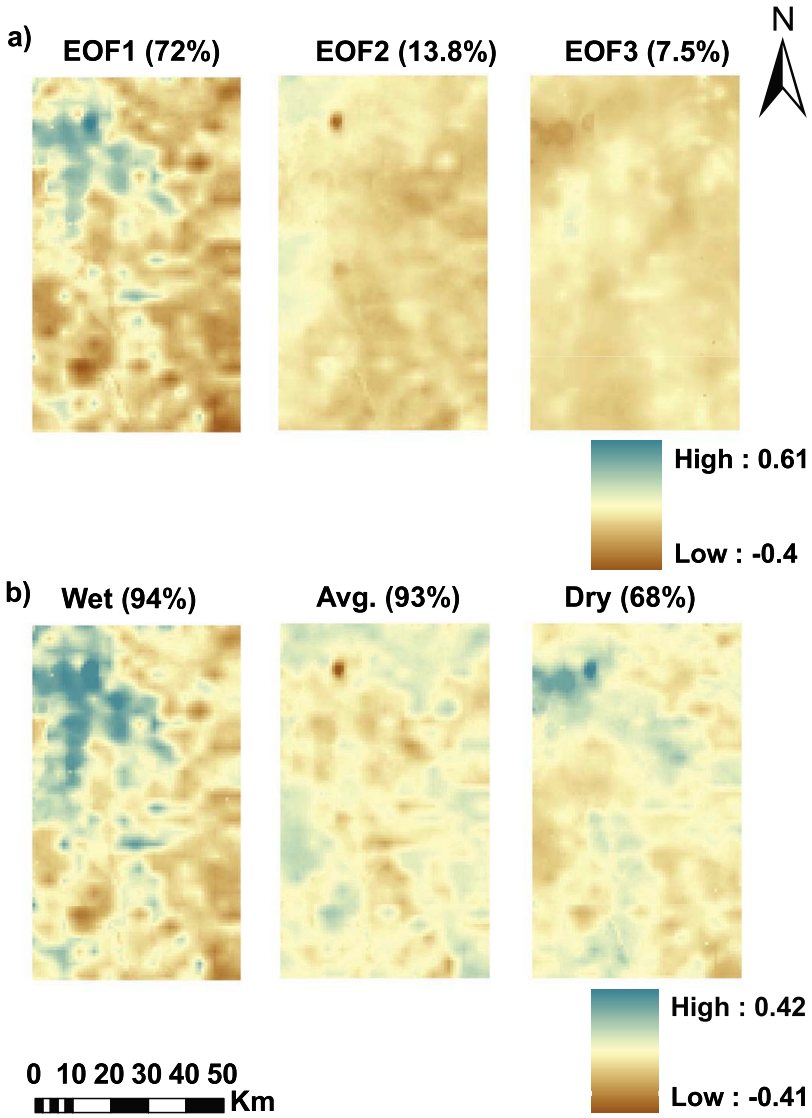

Figure 15. (a) The first three EOFs generated from the spatial anomalies of PSR-derived soil moisture, and the variance explained by each EOF/PC pair. (b) The primary EOFs obtained from wet, average, and dry days at the SMEX02 regional study site in Iowa.

variance explained by them. The associated PC components show the variation in the influence of the EOFs during the wetting/drying phases. The EOF patterns can be further correlated to the geophysical characteristics of the region, such as, precipitation, topography (elevation/slope), soil texture (percent sand/percent clay), landuse/landcover, vegetation parameters, porosity, surface roughness, bulk density, etc. to determine the dominant physical control/s. But the correlations will vary with changing time periods. For example *Jawson and Niemann* [2007] in their study (conducted in the SGP region) found that the primary EOF of soil moisture generated from wet and dry days had the highest correlation with percent sand and percent clay, respectively. They concluded that the highest correlation of the primary EOF with percent sand on wet days is due to the fact that percent sand indicates the ability of a soil to drain faster. Percent clay, on the other hand, indicates the retaining ability of a soil, and consequently, exhibited the highest correlation with the primary EOF on dry days. From our analyses, we inferred that some of the variability of the EOF patterns (generated from soil moisture) is related to topography, soil texture, and rainfall at both the watershed and regional scales in Iowa. But, the impact of rainfall on the soil moisture variability is higher at the watershed scale compared to the regional scale. Furthermore, there is a low correlation at the watershed scale (with few exceptions), and a poor correlation at the regional scale, with respect to the vegetation parameters (VWC, NDVI).

5. Conclusions

[39] We studied the spatiotemporal variability of near-surface soil moisture using both the theta probe measured point-scale soil moisture contents and the remotely sensed pixel-averaged soil moisture fields (~800 m × 800 m) obtained during the Soil Moisture Experiment (SMEX02)

Table 3. Correlations Between the EOFs of Spatial Soil Moisture Anomalies and the Regional Characteristics for the WC Watershed and the SMEX02 Regional Domain in Iowa During SMEX02

Sites	EOFs	Elevation	Slope	% Sand	% Clay	VWC	NDVI	RAIN (EOF1)
WC Watershed (Complete Data Set)	EOF1	−0.185	0.023	0.187	−0.215[a]	0.031	0.056	0.238[a]
	EOF2	0.745[b]	−0.525[b]	−0.541[b]	0.559[b]	−0.338[b]	0.096	−0.696[b]
	EOF3	0.151	−0.091	−0.313[b]	0.267[a]	0.104	0.249[a]	0.156
	EOF4	−0.240[a]	0.261[a]	0.214	−0.200	0.200	−0.145	−0.073
	EOF5	0.414[b]	−0.196	−0.265[a]	0.296[b]	0.062	0.291[b]	−0.020
SMEX02 Regional Site	EOF1	0.359[b]	−0.313[b]	−0.274[b]	0.420[b]	−0.034[b]	−0.073[b]	−0.085[b]
(Complete Data Set)	EOF2	0.198[b]	−0.060[b]	−0.115[b]	0.270[b]	−0.030[b]	−0.032[b]	0.301[b]
	EOF3	−0.030[b]	−0.055[b]	−0.055[b]	−0.027[a]	−0.027[a]	−0.028[a]	0.038[b]
	EOF4	0.596[b]	−0.085[b]	0.041[b]	−0.147[b]	−0.035[b]	−0.028[a]	−0.071[b]
	EOF5	0.216[b]	−0.009	−0.070[b]	0.112[b]	−0.012	−0.045[b]	0.199[b]
	EOF6	0.054[b]	−0.096[b]	−0.051[b]	0.065[b]	−0.046[b]	0.013	−0.064[b]
	EOF7	0.186[b]	−0.062[b]	−0.175[b]	0.028[a]	−0.021	0.086[b]	0.017
WC Watershed	EOF1 (wet)	0.379[b]	−0.344[b]	−0.237[a]	0.229[a]	−0.188[a]	0.105	−0.305[b]
(Wet, Average, and Dry Days)	EOF1 (average)	−0.625[b]	0.364[b]	0.469[b]	−0.506[b]	0.253[a]	0.001	0.679[b]
	EOF1 (dry)	0.512[b]	−0.276[a]	−0.439[b]	0.469[b]	−0.196[a]	0.014	−0.451[b]
SMEX02 Regional Site	EOF1 (wet)	0.383[b]	−0.321[b]	−0.289[b]	0.445[b]	−0.014	−0.079[b]	−0.037[b]
(Wet, Average, and Dry Days)	EOF1 (average)	−0.093[b]	0.198[b]	0.156[b]	−0.161[b]	0.013	0.037[b]	0.208[b]
	EOF1 (dry)	0.228[b]	−0.192[b]	−0.146[b]	0.257[b]	−0.012	−0.029[b]	−0.183[b]

[a]Correlation is significant at the 0.05 significance level.
[b]Correlation is significant at the 0.01 significance level.

conducted in Iowa in 2002, at three different spatial scales: field, watershed and region. At the field scale, theta probe measurements, whereas at the watershed and regional scales, the PSR-derived soil moisture patterns were used for the analyses. However, the volume of surface soil moisture sensed by the C and X band channels of the PSR sensor is smaller compared to the theta probe estimates (~6 cm). A geostatistical analysis (using isotropic semivariograms) was conducted to investigate the evolution of spatial structure and correlation lengths of daily soil moisture fields at different spatial scales. At the field scale (spherical: spatial correlation length ~78–307 m), watershed scale (Gaussian: 2044–11,882 m), and regional scale (exponential: 19,500–118,500 m) model provided a good fit. The correlation lengths increased with decreasing soil moisture content at the field scale as well as within the WC watershed. This may be because of the evolution of different interwinded land surface hydrologic processes and associated dominant geophysical parameters (soil and/or topography) during the dry down sequence. At the SMEX02 regional scale, the trend is opposite with correlation lengths being higher on wet days compared to the dry days. This is because when the soil moisture content is higher following a large storm event, the CV decreases. Some of the previous studies show that with the increase in the soil moisture content, the CV decreases [*Archer et al.*, 1999; *Moran et al.*, 2004]. The decrease in CV due to increasing moisture content may have resulted in higher correlation lengths at the regional study site. The nugget variance is higher at the field scale due to the existing microheterogeneity recorded by the point-scale theta probe measurements. On the other hand, the nugget value is low at the watershed and regional scales for the airborne PSR estimated soil moisture. This may be either due to the measurement/calibration errors, or due to the smoothening of subpixel variability during the soil moisture retrieval process.

[40] Furthermore, the EOF approach was employed to examine the underlying geophysical patterns for determining the different modes of soil moisture variability and the portion of variance explained by each of the mode. At the field scale, it took four EOFs to explain about 81% of the total variability, although the primary EOF (or EOF1) was dominant throughout the observation period compared to the rest of the EOF patterns. At the watershed scale, both EOF1 and EOF2 were dominant, whereas at the regional scale, EOF1 itself explained more than 70% of the variability. Thus, the complicated dynamics of near-surface soil moisture fields can be explained by a few underlying orthogonal spatial structures related to the geophysical attributes of the region. Finally, the relationship between various regional characteristics (rainfall, topography, soil texture, and vegetation) and the EOF patterns was examined to determine the dominant control/s on the soil moisture variability patterns at the watershed and regional scales. EOF analysis was performed on the rainfall data as well, to correlate it with the spatial EOFs generated from soil moisture. Rainfall related primary EOF explained 97% and 88% of the total variance at the watershed and regional scales, respectively. The primary EOFs thus obtained were then correlated with the soil moisture based EOF structures. Results of the correlation analysis showed that rainfall, topography and soil texture have mixed effects on the variability explained by the dominant soil moisture EOFs, at both the watershed and regional scales, while vegetation parameters have limited influence at both spatial scales. The correlation with soil texture may be due to the fact that the dielectric mixing model [*Wang and Schmugge*, 1980] used in the soil moisture retrieval algorithm to estimate the volumetric soil moisture content at each PSR footprint, is based on dominant soil texture information of the footprint. In addition, the reduced effects of vegetation may be due to the use of uniform values of vegetation parameter and single scattering albedo in the retrieval algorithm for all corn and soybean fields, irrespective of their growth stage during the SMEX02 period. The mixed land cover at the PSR footprints may also have contributed toward some of the error in the soil moisture estimates [*Bindlish et al.*, 2006]. Finally, it is evident that rainfall has a higher impact on the soil moisture

variability at the watershed scale compared to the regional scale in Iowa.

[41] **Acknowledgments.** The research was funded by NASA-THP grants (NNX08AF55G and NNX09AK73G) and NSF (CMG/DMS grants CMG-06-21113 and DMS-09-34837). We would like to acknowledge the partial support of USGS for this work. The authors also wish to thank the team of scientists and student participants involved in data collection during the SMEX02 campaign.

References

Archer, F., A. Manu, C. A. Laymon, Z. N. Senwo, and T. L. Coleman (1999), Soil moisture variability on the landscape as a function of land use: Implications for remote sensing of surface soil moisture, *IEEE Trans. Geosci. Remote Sens.*, *2*, 1102–1104.

Bindlish, R., T. J. Jackson, A. J. Gasiewski, M. Klein, and E. G. Njoku (2006), Soil moisture mapping and AMSR-E validation using the PSR in SMEX02, *Remote Sens. Environ.*, *103*(2), 127–139, doi:10.1016/j.rse.2005.02.003.

Charpentier, M. A., and P. M. Groffman (1992), Soil-moisture variability within remote-sensing pixels, *J. Geophys. Res.*, *97*, 18,987–18,995.

Choi, M., and J. M. Jacobs (2007), Soil moisture variability of root zone profiles within SMEX02 remote sensing footprints, *Adv. Water Resour.*, *30*(4), 883–896, doi:10.1016/j.advwatres.2006.07.007.

Cosh, M. H., and W. Brutsaert (1999), Aspects of soil moisture variability in the Washita '92 study region, *J. Geophys. Res.*, *104*, 19,751–19,757.

Cressie, N. A. C. (1993), *Statistics for Spatial Data*, 900 pp., John Wiley, New York.

Crow, W. T., and E. F. Wood (2002), The value of coarse-scale soil moisture observations for regional surface energy balance modeling, *J. Hydrometeorol.*, *3*, 467–482, doi:10.1175/1525-7541(2002)003<0467:TVOCSS>2.0.CO;2.

Das, N. N., and B. P. Mohanty (2008), Temporal dynamics of PSR-based soil moisture across spatial scales in an agricultural landscape during SMEX02: A wavelet approach, *Remote Sens. Environ.*, *112*, 522–534, doi:10.1016/j.rse.2007.05.007.

Delin, S., and K. Berglund (2005), Management zones classified with respect to drought and water logging, *Precis. Agric.*, *6*(4), 321–340, doi:10.1007/s11119-005-2325-4.

De Troch, F. P., P. A. Troch, Z. Su, and D. S. Lin (1996), Application of remote sensing for hydrologic modeling, in *Distributed Hydrologic Modeling*, edited by M. B. Abbott and J. C. Refsgaard, pp. 165–192, Kluwer, Dordrecht, Netherlands.

Drusch, M., and E. F. Wood (1999), Up-scaling effects in passive microwave remote sensing: ESTAR 1.4 GHz measurements during SGP'97, *Geophys. Res. Lett.*, *26*, 879–882.

Dubayah, R., E. F. Wood, and D. Lavalee (1997), Multiscaling analysis in distributed modeling and remote sensing: An application using soil moisture, in *Scaling, Multiscaling, Remote Sensing, and GIS*, edited by M. F. Goodchild and D. A. Quattrochi, pp. 93–111, Cambridge Univ. Press, New York.

Dubois, P. C., J. van Zyl, and T. Engman (1995), Measuring soil moisture with imaging radars, *IEEE Trans. Geosci. Remote Sens.*, *33*, 915–926, doi:10.1109/36.406677.

Entin, J. K., A. Robock, K. Y. Vinnikov, S. E. Hollinger, S. X. Liu, and A. Namkhai (2000), Temporal and spatial scales of observed soil moisture variations in the extratropics, *J. Geophys. Res.*, *105*, 11,865–11,877.

Famiglietti, J. S., J. A. Devereaux, C. A. Laymon, T. Tsegaye, P. R. Houser, T. J. Jackson, S. T. Graham, M. Rodell, and P. J. van Oevelen (1999), Ground-based investigation of soil moisture variability within remote sensing footprints during the Southern Great Plains 1997 (SGP97) Hydrology Experiment, *Water Resour. Res.*, *35*, 1839–1851.

Gordon, H. B., and B. G. Hunt (1987), Interannual variability of the simulated hydrology in a climatic model—Implications for drought, *Clim. Dyn.*, *1*, 113–130, doi:10.1007/BF01054480.

Grayson, R. B., and A. W. Western (1998), Towards areal estimation of soil water content from point measurements: Time and space stability of mean response, *J. Hydrol. Amsterdam*, *207*(1–2), 68–82, doi:10.1016/S0022-1694(98)00096-1.

Hills, T. C., and S. G. Reynolds (1969), Illustrations of soil moisture variability in selected areas and plots of different sizes, *J. Hydrol. Amsterdam*, *8*, 27–47, doi:10.1016/0022-1694(69)90029-8.

Hu, Z. L., S. Islam, and Y. Cheng (1997), Statistical characterization of remotely sensed soil moisture images, *Remote Sens. Environ.*, *61*(2), 310–318, doi:10.1016/S0034-4257(97)89498-9.

Issaks, E. H., and R. M. Srivastava (1989), *An Introduction to Applied Geostatistics*, 561 pp., Oxford Univ. Press, New York.

Jackson, T. J. (1993), Measuring surface soil moisture using passive microwave remote sensing. III, *Hydrol. Processes*, *7*(2), 139–152, doi:10.1002/hyp.3360070205.

Jackson, T. J., and D. E. Le Vine (1996), Mapping surface soil moisture using an aircraft-based passive microwave instrument: Algorithm and example, *J. Hydrol. Amsterdam*, *184*, 85–99, doi:10.1016/0022-1694(95)02969-9.

Jackson, T. J., and T. J. Schmugge (1995), Surface soil-moisture measurement with microwave radiometry, *Acta Astronaut.*, *35*(7), 477–482, doi:10.1016/0094-5765(94)00288-W.

Jackson, T. J., D. M. Le Vine, C. T. Swift, T. J. Schmugge, and F. R. Schiebe (1995), Large-area mapping of soil-moisture using the ESTAR passive microwave radiometer in Washita'92, *Remote Sens. Environ.*, *54*(1), 27–37, doi:10.1016/0034-4257(95)00084-E.

Jacobs, J. M., B. P. Mohanty, E.-C. Hsu, and D. Miller (2004), SMEX02: Field scale variability, time stability and similarity of soil moisture, *Remote Sens. Environ.*, *92*, 436–446, doi:10.1016/j.rse.2004.02.017.

Jawson, S. D., and J. D. Niemann (2007), Spatial patterns from EOF analysis of soil moisture at a large scale and their dependence on soil, land-use, and topographic properties, *Adv. Water Resour.*, *30*(3), 366–381, doi:10.1016/j.advwatres.2006.05.006.

Jolliffe, I. T. (2002), *Principal Component Analysis*, 487 pp., Springer, New York.

Journel, A. G., and C. J. Huijbregts (1978), *Mining Geostatistics*, 600 pp., Academic, San Diego, Calif.

Kerr, Y. H. (2007), Soil moisture from space: Where are we?, *Hydrogeol. J.*, *15*, 117–120, doi:10.1007/s10040-006-0095-3.

Kim, G., and A. P. Barros (2002a), Downscaling of remotely sensed soil moisture with a modified fractal interpolation method using contraction mapping and ancillary data, *Remote Sens. Environ.*, *83*(3), 400–413, doi:10.1016/S0034-4257(02)00044-5.

Kim, G., and A. P. Barros (2002b), Space-time characterization of soil moisture from passive microwave remotely sensed imagery and ancillary data, *Remote Sens. Environ.*, *81*(2–3), 393–403, doi:10.1016/S0034-4257(02)00014-7.

Merlin, O., A. Chehbouni, Y. H. Kerr, and D. C. Goodrich (2006), A downscaling method for distributing surface soil moisture within a microwave pixel: Application to the Monsoon '90 data, *Remote Sens. Environ.*, *101*(3), 379–389, doi:10.1016/j.rse.2006.01.004.

Merlin, O., J. P. Walker, A. Chehbouni, and Y. H. Kerr (2008), Towards deterministic downscaling of SMOS soil moisture using MODIS derived soil evaporative efficiency, *Remote Sens. Environ.*, *112*(10), 3935–3946, doi:10.1016/j.rse.2008.06.012.

Mohanty, B. P., and T. H. Skaggs (2001), Spatio-temporal evolution and time-stable characteristics of soil moisture within remote sensing footprints with varying soil, slope, and vegetation, *Adv. Water Resour.*, *24*, 1051–1067, doi:10.1016/S0309-1708(01)00034-3.

Mohanty, B. P., J. S. Shouse, and M. T. van Genuchten (1998), Spatio-temporal dynamics of water and heat in a field soil, *Soil Tillage Res.*, *47*(1–2), 133–143, doi:10.1016/S0167-1987(98)00084-1.

Mohanty, B. P., J. S. Famiglietti, and T. H. Skaggs (2000), Evolution of soil moisture spatial structure in a mixed vegetation pixel during the Southern Great Plains 1997(SGP97) Hydrology Experiment, *Water Resour. Res.*, *36*, 3675–3686.

Moran, M. S., C. D. Peters-Lidard, J. M. Watts, and S. McElroy (2004), Estimating soil moisture at the watershed scale with satellite-based radar and land surface models, *Can. J. Rem. Sens.*, *30*(5), 805–826.

Njoku, E. G., T. J. Jackson, V. Lakshmi, T. K. Chan, and S. V. Nghiem (2003), Soil moisture retrieval from AMSR-E, *IEEE Trans. Geosci. Remote Sens.*, *41*(2), 215–229, doi:10.1109/TGRS.2002.808243.

Nyberg, L. (1996), Spatial variability of soil water content in the covered catchment at Gårdsjön, Sweden, *Hydrol. Processes*, *10*(1), 89–103, doi:10.1002/(SICI)1099-1085(199601)10:1<89::AID-HYP303>3.0.CO;2-W.

Perry, M. A., and J. D. Niemann (2007), Analysis and estimation of soil moisture at the catchment scale using EOFs, *J. Hydrol. Amsterdam*, *334*(3–4), 388–404, doi:10.1016/j.jhydrol.2006.10.014.

Piepmeier, J. R., and A. J. Gasiewski (2001), High-resolution passive polarimetric microwave mapping of ocean surface wind vector fields, *IEEE Trans. Geosci. Remote Sens.*, *39*(3), 606–622, doi:10.1109/36.911118.

Preisendorfer, R. W. (1988), *Principal Component Analysis in Meteorology and Oceanography*, 425 pp., Elsevier, New York.

Ryu, D., and J. S. Famiglietti (2006), Multi-scale spatial correlation and scaling behavior of surface soil moisture, *Geophys. Res. Lett.*, *33*, L08404, doi:10.1029/2006GL025831.

Schmugge, T. J. (1998), Applications of passive microwave observations of surface soil moisture, *J. Hydrol. Amsterdam*, *212–213*, 188–197, doi:10.1016/S0022-1694(98)00209-1.

Schmugge, T. J., and T. J. Jackson (1996), Soil moisture variability, in *Scaling-up in Hydrology Using Remote Sensing*, edited by J. B. Stewart et al., pp. 183–192, Wiley, Chichester, U. K.

Starr, G. C. (2005), Assessing temporal stability and spatial variability of soil water patterns with implications for precision water management, *Agric. Water Manage.*, *72*(3), 223–243, doi:10.1016/j.agwat.2004.09.020.

Ulaby, F. T., P. C. Dubois, and J. van Zyl (1996), Radar mapping of surface soil moisture, *J. Hydrol. Amsterdam*, *184*, 57–84, doi:10.1016/0022-1694(95)02968-0.

Wackernagel, H. (2003), *Multivariate Geostatistics*, 387 pp., Springer, New York.

Wang, J. R., and T. J. Schmugge (1980), An empirical model for the complex dielectric permittivity of soils as a function of water content, *IEEE Trans. Geosci. Remote Sens.*, *18*, 288–295, doi:10.1109/TGRS.1980.350304.

Warrick, A. W., R. Zhang, M. M. Moody, and D. E. Meyers (1990), Kriging versus alternative interpolators: Errors and sensitivity to model inputs, in *Field-scale water and solute flux in soils*, edited by K. Roth et al., pp. 157–164, Birkhäuser Boston, Cambridge, Mass.

Western, A. W., and G. Blöschl (1999), On the spatial scaling of soil moisture, *J. Hydrol. Amsterdam*, *217*, 203–224, doi:10.1016/S0022-1694(98)00232-7.

Western, A. W., G. Blöschl, and R. B. Grayson (1998), Geostatistical characterization of soil moisture patterns in the Tarrawarra a catchment, *J. Hydrol. Amsterdam*, *205*(1–2), 20–37, doi:10.1016/S0022-1694(97)00142-X.

Western, A. W., S. L. Zhou, R. B. Grayson, T. A. McMahon, G. Blöschl, and D. J. Wilson (2004), Spatial correlation of soil moisture in small catchments and its relationship to dominant spatial hydrological processes, *J. Hydrol. Amsterdam*, *286*(1–4), 113–134, doi:10.1016/j.jhydrol.2003.09.014.

Yoo, C., and S. Kim (2004), EOF analysis of surface soil moisture field variability, *Adv. Water Resour.*, *27*(8), 831–842, doi:10.1016/j.advwatres.2004.04.003.

C. Joshi and B. P. Mohanty, Department of Biological and Agricultural Engineering, Texas A&M University, 2117 TAMU; 201 Scoates Hall, College Station, TX 77843, USA. (bmohanty@tamu.edu)